

Folding of Horse Cytochrome *c* in the Reduced State

Abani K. Bhuyan^{1*} and Jayant B. Udgaonkar²

¹*School of Chemistry
University of Hyderabad
Hyderabad 500046, India*

²*National Center for Biological
Sciences, UAS-GKVK Campus
Bangalore 560065, India*

Equilibrium and kinetic folding studies of horse cytochrome *c* in the reduced state have been carried out under strictly anaerobic conditions at neutral pH, 10 °C, in the entire range of aqueous solubility of guanidinium hydrochloride (GdnHCl). Equilibrium unfolding transitions observed by Soret heme absorbance, excitation energy transfer from the lone tryptophan residue to the ferrous heme, and far-UV circular dichroism (CD) are all biphasic and superimposable, implying no accumulation of structural intermediates. The thermodynamic parameters obtained by two-state analysis of these transitions yielded $\Delta G(\text{H}_2\text{O}) = 18.8(\pm 1.45)$ kcal mol⁻¹, and $C_m = 5.1(\pm 0.15)$ M GdnHCl, indicating unusual stability of reduced cytochrome *c*. These results have been used in conjunction with the redox potential of native cytochrome *c* and the known stability of oxidized cytochrome *c* to estimate a value of -164 mV as the redox potential of the unfolded protein. Stopped-flow kinetics of folding and unfolding have been recorded by Soret heme absorbance, and tryptophan fluorescence as observables. The refolding kinetics are monophasic in the transition region, but become biphasic as moderate to strongly native-like conditions are approached. There also is a burst folding reaction unobservable in the stopped-flow time window. Analyses of the two observable rates and their amplitudes indicate that the faster of the two rates corresponds to apparent two-state folding ($U \leftrightarrow N$) of 80-90% of unfolded molecules with a time constant in the range 190-550 μs estimated by linear extrapolation and model calculations. The remaining 10-20% of the population folds to an off-pathway intermediate, *I*, which is required to unfold first to the initial unfolded state, *U*, in order to refold correctly to the native state, *N* ($I \leftrightarrow U \leftrightarrow N$). The slower of the two observable rates, which has a positive slope in the linear functional dependence on the denaturant concentration indicating that an unfolding process under native-like conditions indeed exists, originates from the unfolding of *I* to *U*, which rate-limits the overall folding of these 10-20% of molecules. Both fast and slow rates are independent of protein concentration and pH of the refolding milieu, suggesting that the off-pathway intermediate is not a protein aggregate or trapped by heme misligation. The nature or type of unfolded-state heme ligation does not interfere with refolding. Equilibrium pH titration of the unfolded state yielded coupled ionization of the two non-native histidine ligands, H26 and H33, with a pK_a value of 5.85. A substantial fraction of the unfolded population persists as the six-coordinate form even at low pH, suggesting ligation of the two methionine residues, M65 and M80. These results have been used along with the known ligand-binding properties of unfolded cytochrome *c* to propose a model for heme ligation dynamics. In contrast to refolding kinetics, the unfolding kinetics of reduced cytochrome *c* recorded by observation of Soret absorbance and tryptophan fluorescence are all slow, simple, and single-exponential. In the presence of 6.8 M GdnHCl, the unfolding time constant is $\sim 300(\pm 125)$ ms. There is no burst unfolding reaction. Simulations of the observed folding-unfolding kinetics by numerical solutions of the rate equations corresponding to the three-state $I \leftrightarrow U \leftrightarrow N$ scheme have yielded the microscopic rate constants.

Abbreviations used: cyt, cytochrome; ferricyt, ferricytochrome; ferrocyt, ferrocycytochrome; GdnHCl, guanidinium hydrochloride; HX, hydrogen exchange; NAM, *N*-acetyl-DL-methionine.

E-mail address of the corresponding author: akbcs@uohyd.ernet.in

*Corresponding author

Keywords: oxidized and reduced cytochrome *c*; ferrocycytochrome *c*; unfolded state; heme axial ligation; ligand exchange dynamics

Introduction

The argument following Levinthal that if specific kinetic pathways were not available, and instead the unfolded polypeptide had to arrange itself in a random search for the energy minimum, folding could not occur in seconds or less, is rational and even appears justified for some proteins that fold *via* discrete kinetic intermediates within the formalism of classical pathway models.^{1,2} Some proteins, on the other hand, fold in a two-state manner without engaging detectable intermediates,³ raising questions concerning the existence and accumulation, and the necessity of folding intermediates. The folding pathway model advocates for the involvement of discrete intermediates, and insists that they are necessary to guide the polypeptide to the native state. The accumulation of such intermediate structures to a level detectable experimentally depends on their lifetime and energetic stability. The new models of protein folding, theoretical in nature, at the other end, picture a continuum of ensembles of intermediate structures rather than discrete ones, and do not consider them necessary for the unfolded polypeptide ensemble to achieve the native state. Also, the accumulation of an ensemble of folding structures to a detectable level is seen as a consequence of the ruggedness of the energy landscape. When the landscape is sufficiently smooth, folding occurs in a two-state manner without accumulation of intermediates. Thus, the two models agree upon conditional accumulation of intermediates, but contest the necessity for them.

The necessity of discrete folding structures is, in fact, the central theme of the classical pathway model. If such well-defined intermediate structures indeed compose the folding-unfolding pathways, as viewed by the pathway model, then, by corollary, they must be on-pathway, and thus productive. The possibility of an unproductive role of kinetic intermediates, however, has also been considered (e.g. see Ikai & Tanford⁴), but has received little attention because of the lack of direct experimental observation of off-pathway structures, and because the off-pathway nature leads to a dead-end, and hence does not shed light on the folding mechanism. Theoretical models, of course, do not attach importance to the pathway nature of the folding reaction. Any folding ensemble that does not monotonically increase native-like resemblance on the folding run may be considered off-pathway.⁵

We have studied the equilibrium and kinetic aspects of folding of horse cytochrome *c* (cyt *c*) in the reduced state to examine the protein stability,

the speed of folding, and the involvement and the pathway nature of intermediate structures. Horse cyt *c*, being small and monomeric, and by the virtue of possessing a single tryptophan residue and a heme moiety, has been amenable to measurement by the use of a large number of physical methods. Indeed, numerous reports of chain folding of cyt *c* with the heme iron in the oxidized state (oxidized cytochrome *c* or ferricytochrome *c*) have appeared during the past 30 years.⁶⁻¹⁹ On the other hand, folding studies of the reduced form of horse cyt *c* (reduced cyt *c* or ferrocyt *c*) have been scanty even though the post-translational folding of cyt *c* is likely to occur in the reduced form in the highly reductive intracellular milieu. Observations on the reduced form have been limited to equilibrium denaturation,²⁰⁻²⁴ and heme absorbance-monitored kinetic measurements in a narrow range of denaturant concentration.^{20,22,25,26} Furthermore, none of these reports has provided any information about the progress of kinetic amplitude, the measurement of which is often rendered difficult by the extreme oxygen-sensitivity of denatured ferrocyt *c*. By using heme absorbance in the Soret region, tryptophan fluorescence, and far-UV CD as probes for equilibrium unfolding, and Soret absorbance and tryptophan fluorescence for stopped-flow kinetic experiments, we have now measured the folding-unfolding reaction of reduced cyt *c* over the entire possible range of guanidinium hydrochloride (GdnHCl) concentration by paying close attention to observable signals. This article reports on a detailed quantitative measurement of the folding reaction of ferrocyt *c* carried out in an oxygen-free atmosphere under well-controlled solution conditions. It is known that the folding kinetics of oxidized cyt *c* is interfered with by ligation of non-native heme ligands in the unfolded state,¹⁴ and thus appears, to some investigators, as a paradigm of kinetic misfolding. We have made considerable effort to show that such is not the case with reduced cyt *c*.

The results show a simple two-state equilibrium transition for the unfolding of ferrocyt *c* irrespective of the probe used. The protein stability has been correlated with the known redox potential of cyt *c*. We find fast refolding of 80-90% of molecules ($\tau \sim 190-550 \mu\text{s}$) without accumulation of a kinetic intermediate. The remaining 10-20% of molecules fold to an off-pathway intermediate that unfolds back to the initial unfolded state in order to refold to the native state. This segregation of the refolding population has been suggested to take place during kinetic partitioning at the incipient phase of refolding. The segregation is independent of both protein concentration and the nature of

heme ligation in the unfolded chains. Further, the heme-ligand dynamics have been shown not to interfere with refolding. Since the refolding kinetics are insensitive to both the pH of the refolding medium and the concentration of protein, the formation and accumulation of I is not related to heme misligation-facilitated arrest of folding or to protein aggregation. A classical three-state off-pathway model, $I \leftrightarrow U \leftrightarrow N$, simulates the available result.

Results

Optical spectra of ferrocycytochrome *c* in native and unfolded states

To introduce the various spectral probes used in this study we first present the equilibrium spectra of ferrocycytochrome *c* in native and unfolded states. Figure 1(a) shows the solution-state Soret spectra of native and unfolded ferrocycytochrome *c* at 20 °C. The native state Soret band ($\lambda_{\text{max}} = 415 \text{ nm}$, $\epsilon = 125 \text{ mM}^{-1} \text{ cm}^{-1}$) has been assigned to a porphyrin $\pi \rightarrow \pi^*$ ($a_{1u}, a_{2u} \rightarrow e_g$) optical transition.²⁷ Unfolding results in a red shift of the Soret band to 418 nm, and ϵ attains a new value of $103 \text{ mM}^{-1} \text{ cm}^{-1}$. The shoulder in the unfolded-state spectrum centered around 428 nm represents, most likely, a small fraction of five-coordinate heme in the unfolded state. The changes in the heme absorption spectrum upon unfolding result from changes in heme symmetry. The crystal field symmetry of the heme is determined by the constraints imposed on it by heme-polypeptide interactions *via* the heme axial ligands and by the spatial structure around it. In native cyt *c*, the heme axial ligation of H18 and M80, and the distortion of the planar heme geometry into a saddle shape,²⁸ whereby electronic equivalence of the four iron-bonded porphyrin nitrogen atoms is lifted, lowers the heme symmetry from tetragonal to rhombic. When cyt *c* unfolds, the heme-protein interactions are altered with the loss of the M80 ligand, causing a decrease in the magnitude of rhombicity but an increase in tetragonality. It is this shift in the heme geometry and the consequent changes in the crystal field symmetry that is manifested in changes in the porphyrin $\pi \rightarrow \pi^*$ transitions during protein unfolding. The difference spectrum of native and unfolded state spectra (Figure 1(a), inset) shows a positive band at 411 nm and a negative band at 430 nm, both of which have been used extensively to monitor the equilibrium and kinetics of ferrocycytochrome *c* folding reported here. Unfolding of ferrocycytochrome *c* also produces significant changes in band positions and associated values of ϵ in the visible and near-infrared regions (data not shown). The properties of these transitions can often be exploited to learn finer details of folding mechanism.

Figure 1(b) shows steady-state tryptophan fluorescence spectra in native and unfolded states. In the native structure, the fluorescence of W59 is quenched almost completely due to excitation

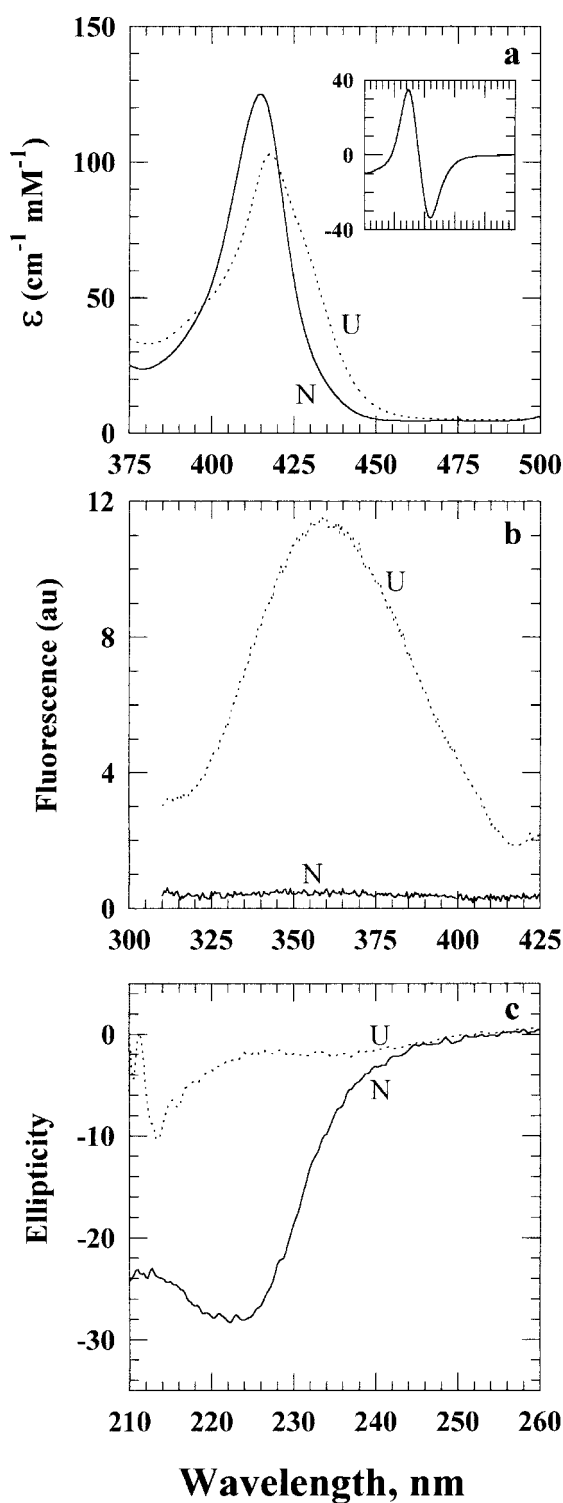


Figure 1. Spectral changes accompanying unfolding of ferrocycytochrome *c*. (a) Soret absorbance: unfolding results in a red shift of the Soret band from 415 nm to 418 nm. The peak wavelengths in the difference spectrum of native and unfolded ferrocycytochrome *c* (6.3 M GdnHCl), shown in the inset, are 411 nm (positive) and 430 nm (negative). (b) Tryptophan fluorescence: the native protein does not fluoresce, and the wavelength of maximum emission in the unfolded state (7.7 M GdnHCl) upon excitation at 280 nm is 358 nm. (c) Far-UV CD spectra of native and unfolded ferrocycytochrome *c*.

energy transfer to the heme.²⁹ Unfolding results in an increase in the heme-tryptophan distance, and hence a dramatic increase in the fluorescence quantum yield,^{18,29–31} with the emission peak, λ_{em} , centered around 357 nm. The λ_{em} does not shift with increasing concentrations of denaturant even though the emission intensity in the unfolded state increases linearly with molar concentration of GdnHCl. The fluorescence at ~ 357 nm can thus be used to monitor the global structural transition of ferrocyst *c* across the N \leftrightarrow U equilibrium. These fluorescence properties of cyt *c* are independent of the heme oxidation state and, as documented in numerous studies,^{9,15,30} are applicable to folding studies of ferrocyst *c* as well.

Peptide CD spectra of native and unfolded ferrocyst *c* are shown in Figure 1(c) and, as for other proteins, the loss of secondary structure leads to a decrease in peptide ellipticity. Here, only the equilibrium transition measured by CD has been presented. High-precision kinetic data were difficult to acquire due to little signal amplitude observed under strongly native-like conditions. Further, the noise is amplified by the presence of a slight excess of sodium dithionite that absorbs strongly in the peptide region.

Equilibrium unfolding of ferrocystochrome *c*

To examine the protein stability and the thermodynamic properties of the N \leftrightarrow U reaction, GdnHCl-induced equilibrium unfolding of ferrocyst *c* was studied by using all spectroscopic probes outlined above. Figure 2(a) shows the 430 nm absorbance of ferrocyst *c* as a function of GdnHCl concentration. The Soret spectra recorded at each concentration of GdnHCl yield absorbance values at both 430 and 411 nm (see Figure 1(a)). The data shown for 430 nm have been normalized with respect to the absorbance value in the presence of 7.3 M GdnHCl, and the continuous line represents the iterated fit to equation (1). The fit parameters, namely, $\Delta G(H_2O)$, m_g , and C_m ($\cong \Delta G(H_2O)/m_g$), are given in the legend to Figure 2. Identical fit parameters are obtained with the absorbance values at 411 nm (data not shown).

Figure 2(b) shows the steady-state fluorescence intensity of reduced cyt *c* as a function of GdnHCl. Structural unfolding in the transition region produces a sharp increase in tryptophan fluorescence, but the fluorescence continues to increase monotonously even after the major unfolding transition is complete. This increase, observed also in the oxidized state of cyt *c*,^{15,18,30} results from a continuous increase in the average heme-tryptophan distance due to expansion of the unfolded chain. The GdnHCl-dependence of fluorescence values in the Figure has been normalized with respect to the fluorescence intensity in the presence of 7.8 M GdnHCl. The continuous line is the fit of the data to equation (1), and the fit parameters are given in the legend to Figure 2.

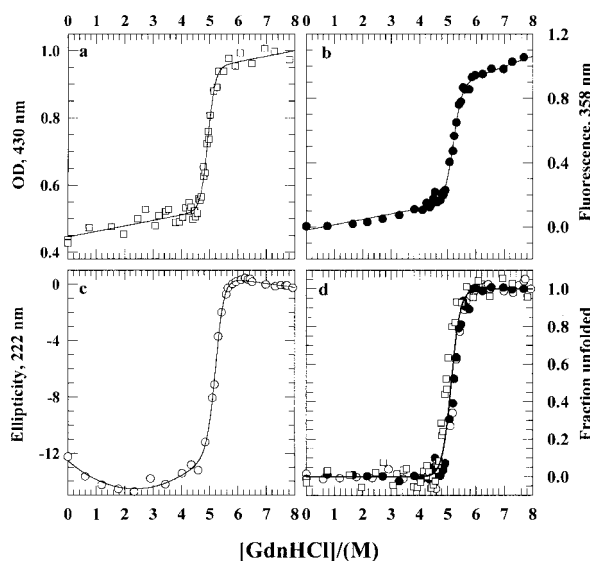


Figure 2. GdnHCl-induced equilibrium unfolding of reduced cyt *c* at 10°C, neutral pH, monitored by (a) Soret absorbance at 430 nm, (b) tryptophan fluorescence at 358 nm on excitation at 280 nm, and (c) far-UV CD. The curves are least-squares fits to the data using a two-state model according to equation (1). (c) The native-state baseline of CD data are approximated by $\theta = c_f + m_1[\text{GdnHCl}] + m_2[\text{GdnHCl}]^2$. Values of ΔG and m_g , respectively, are: (a) $21.8(\pm 0.2)$ kcal mol⁻¹ and $4.4(\pm 0.2)$ kcal mol⁻¹ M⁻¹ for absorbance at 430 nm; (b) $19.3(\pm 0.5)$ kcal mol⁻¹ and $3.7(\pm 0.2)$ kcal mol⁻¹ M⁻¹ for fluorescence; and (c) $20.4(\pm 0.3)$ kcal mol⁻¹ and $3.8(\pm 0.1)$ kcal mol⁻¹ M⁻¹ for far-UV CD. (d) The data from (a), (b), and (c) are plotted as fraction unfolded as a function of GdnHCl concentration. All three sets of normalized data were fit simultaneously to equation (2), which yielded values for $\Delta G(H_2O) = 18.8(\pm 1.45)$ kcal mol⁻¹, $m_g = 3.7(\pm 0.23)$ kcal mol⁻¹ M⁻¹, and $C_m = 5.1$ M GdnHCl.

The GdnHCl concentration-dependence of the peptide ellipticity signal is shown in Figure 2(c). Unlike the linear dependence on GdnHCl concentration of Soret absorbance and fluorescence values in the native baseline region, the CD signals show a pronounced curvature before the sharp signal loss in the global transition region. To account for this feature, a second-order polynomial was used to approximate the native baseline in equation (1). The iterated fit parameters thus obtained are given in the Figure legend. If a linear dependence of CD signal on GdnHCl concentration in the native baseline region is assumed, then the value of $\Delta G(H_2O)$ is found to be less by 3.5 kcal mol⁻¹ (1 cal = 4.184 J).

The equilibrium unfolding behavior measured by these three probes is compared in Figure 2(d) by plotting the normalized fraction of protein unfolded as a function of GdnHCl concentration. The thermodynamic parameters obtained by fitting the three combined data sets to equation (2) are

$\Delta G(\text{H}_2\text{O}) \approx 18.8 (\pm 1.45) \text{ kcal mol}^{-1}$, and $m_g \approx 3.7 (\pm 0.23) \text{ kcal mol}^{-1} \text{ M}^{-1}$. Here, we use these values to indicate the thermodynamic stability of the protein. The monophasic nature of the transition displayed by each of the three sets of equilibrium data and the coincidence of the three transitions indicate that under equilibrium conditions the $\text{N} \leftrightarrow \text{U}$ reaction of ferrocyst *c* is a two-state cooperative process with no accumulation of intermediate structures.

Folding and unfolding kinetics of ferrocystochrome *c*

Kinetic traces

Since a single observable often is insufficient to obtain a more comprehensive picture of the kinetic mechanism of protein conformational changes, we used three probes, namely, Soret heme absorbance at 411 and 430 nm, and tryptophan fluorescence, to record the folding and unfolding kinetics of ferrocyst *c* in several series of stopped-flow experiments, all done at 10 °C and neutral pH. Figure 3 shows a few kinetic traces recorded by Soret heme absorbance. In the presence of 1.05 M GdnHCl, the refolding course observed at 430 nm is best described by two exponentials, a fast process with an apparent rate, λ_1 , of 140 s^{-1} , and a slow process with λ_2 of 2.6 s^{-1} (Figure 3(a) and the inset). Relative amplitudes corresponding to the two processes are 0.83 and 0.17, respectively. All traces of refolding in less than $\sim 2 \text{ M}$ GdnHCl were fitted satisfactorily by two phases, and the distribution of amplitudes for the fast and the slow phases followed a $0.85(\pm 0.05):0.15(\pm 0.05)$ ratio (Figure 3(b) inset). The traces plotted in Figure 3(b), normalized with reference to the signal of the unfolded protein, show that a major fraction of the signal is already recovered within the dead-time of the instrument. This signal loss, also called missing amplitude or burst phase amplitude, has a strong dependence on the final concentration of GdnHCl in the refolding milieu; the lower the final denaturant concentration, the larger the recovery.

At 411 nm, however, the observed folding course is monophasic. All traces shown in Figure 3(c) can be fit to a single-exponential function, and for the same final concentration of GdnHCl, the single rate measured at 411 nm is very similar in magnitude to the faster rate (λ_1) measured at 430 nm. The unfolding kinetics recorded at both Soret wavelengths (not shown) are satisfactorily described by a single kinetic phase, and the total expected amplitude is observed entirely, even under strongly unfolding conditions.

Displayed in Figure 4 are samples of fluorescence-observed kinetic traces for folding and unfolding. Figure 4(a) shows that when refolded from $\sim 7 \text{ M}$ to 0.85 M GdnHCl, the fluorescence decays in two observable kinetic phases: a fast phase with an apparent rate constant, $\lambda_1 = 165 \text{ s}^{-1}$,

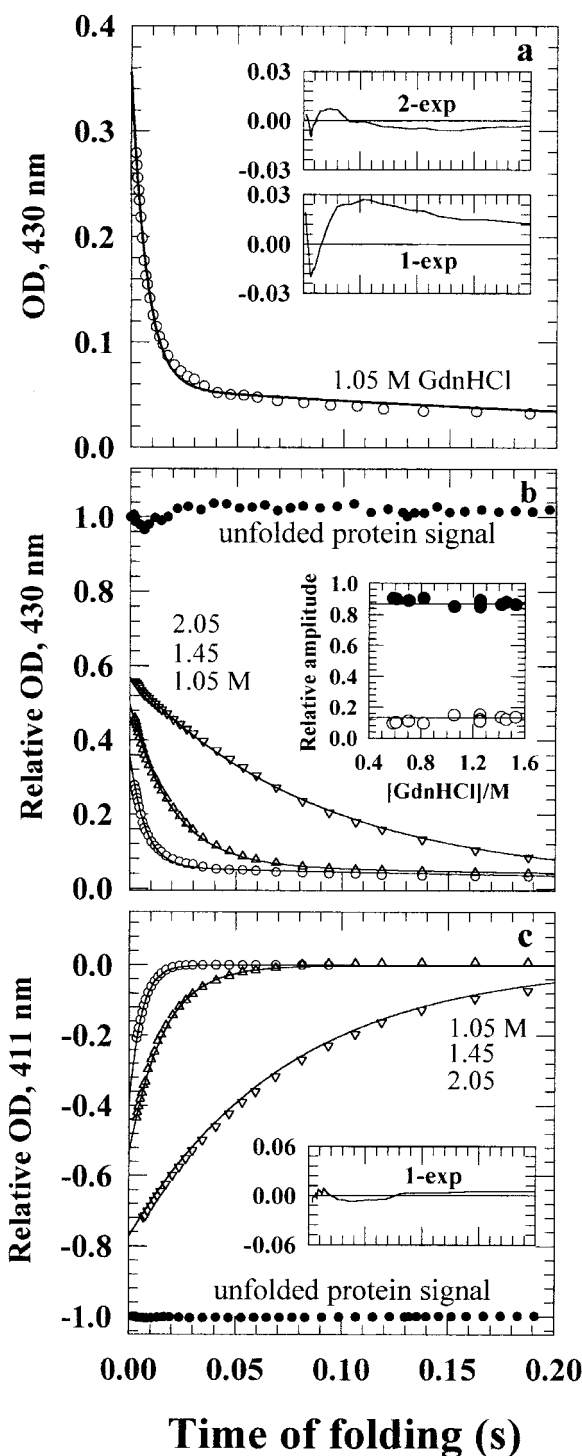
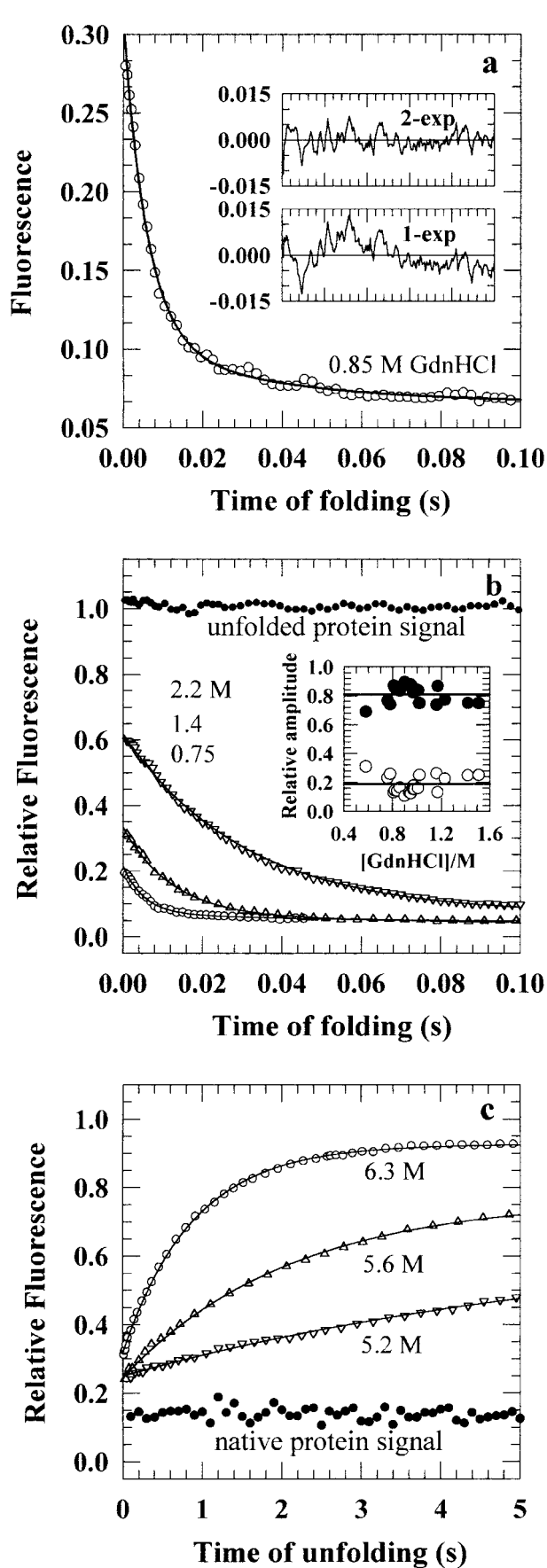


Figure 3. Soret heme absorbance-monitored refolding. (a) Biphasic kinetics when refolded to strongly native-like conditions (shown for 1.05 M GdnHCl), monitored at 430 nm. The inset shows residuals from one and two-exponential fits of the data. (b) A large fraction of the 430 nm signal is recovered during a burst phase of the folding reaction. The inset shows the averaged distribution of 0.87:0.13 of observable amplitudes of the major (●) and the minor (○) phase in GdnHCl concentrations less than $\sim 1.6 \text{ M}$. (c) Refolding traces recorded at 411 nm can be fitted using a single exponential (inset). There is a pronounced burst signal amplitude akin to kinetics monitored at 430 nm.



and a slow phase characterized by $\lambda_2 = 22 \text{ s}^{-1}$. The residuals obtained from single and double-exponential fits to the kinetic data show that the second half of the data are fit much better by the latter than the former (Figure 4(a), inset). Figure 4(b) presents three representative kinetic traces for folding under strongly native-like conditions. Two-exponential folding kinetics are seen for refolding in GdnHCl concentrations below $\sim 1.5 \text{ M}$, and the relative amplitudes of the two phases are $0.8(\pm 0.1)$ and $0.2(\pm 0.1)$ for the fast and the slow phase corresponding to λ_1 and λ_2 , respectively (Figure 4(b), inset). The display of kinetic traces normalized with reference to the fluorescence signal of the unfolded protein (Figure 4(b)) also indicates that a fraction of the total expected fluorescence signal is lost within the dead-time of the kinetic spectrometer; the lower the denaturant concentration, the greater the loss. These fluorescence-monitored kinetics are similar to those observed by Soret heme absorbance at 430 nm (Figure 3(a)). In contrast to the complex folding behavior, the fluorescence-monitored unfolding course is slow and appears simple. The normalized kinetic traces shown in Figure 4(c) indicate that the unfolding process under the present conditions occurs in a single, completely observable rise of fluorescence irrespective of the final concentration of GdnHCl.

The chevrons

Figure 5(a) presents the denaturant-dependence of the logarithm of the observed folding and unfolding rates measured by Soret heme absorbance. For the equilibrium $\text{N} \leftrightarrow \text{U}$ transition of ferrocyst *c*, the transition midpoint, C_m , is $\approx 5 \text{ M}$ GdnHCl (Figure 2(a) and (d)), which corresponds to the relaxation minimum in the chevron plot. Expectedly, the rate of the single observable folding phase increases progressively as the GdnHCl concentration in the reaction medium is lowered below the transition midpoint. In denaturant concentrations below $\sim 1.5 \text{ M}$, a new feature emerges

Figure 4. Representative stopped-flow kinetic traces of ferrocyst *c* refolding monitored by tryptophan fluorescence at 10°C , neutral pH. (a) When refolded under strongly native-like conditions (shown here for 0.85 M GdnHCl), refolding occurs in two kinetic phases. The insets show residuals from one and two-exponential fits. (b) Traces showing recovery of signal amplitudes (normalized with respect to the fluorescence signal of the unfolded protein) during the burst kinetic phase. The burst amplitude increases as the denaturant concentration in the refolding medium is lowered. The inset shows $\sim 0.8:0.2$ distribution of observable amplitudes of the major (●) and the minor (○) phase in GdnHCl concentrations less than $\sim 1.6 \text{ M}$. (c) Unfolding traces to show the single unfolding kinetic phase without any appreciable burst unfolding. The continuous lines through the traces represent non-linear least-squares best fits of the data.

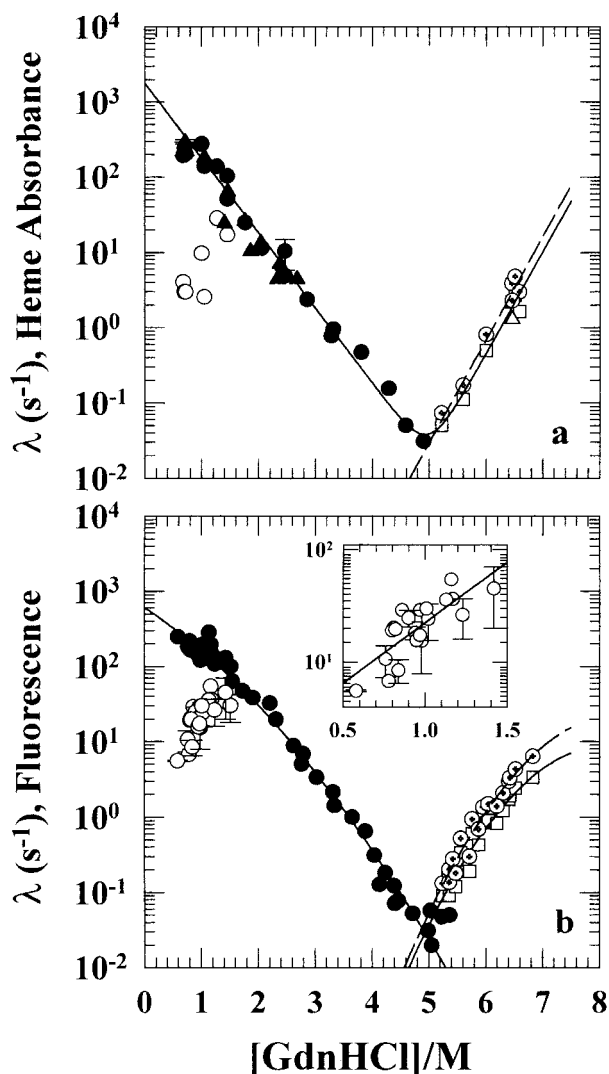


Figure 5. Dependence of apparent rates of folding and unfolding on denaturant concentration. (a) Soret heme absorbance: at 430 nm, major folding phase (●) minor folding phase (○) and the unfolding phase (□); and at 411 nm, the single folding phase (▲) and the unfolding phase (△). (b) Tryptophan fluorescence: major folding phase (●) minor folding phase (○) and the unfolding phase (□). The continuous line in (b) has been drawn using polynomial fits as described in the text. The fit of data in (a) is according to equations (4). The relevant fit parameters in each case are listed in Table 1. The open circles with crosshair (⊕) in both panels are the apparent rates of unfolding corrected for the effect of intrinsic viscosity of GdnHCl (see the text), and the broken lines through them have been drawn according to linear rate-denaturant relation (absorbance data in (a)) and polynomial fit (fluorescence data in (b)).

in the chevron (see Figure 3 also): the folding time-course observed at 430 nm decays in two phases, the relative amplitudes of which are ~ 0.85 and ~ 0.15 for the fast and the slow phase, respectively. This distribution of the observable amplitudes at

430 nm is a constant for all biphasic folding courses observed in the presence of a denaturant concentration less than ~ 1.5 M GdnHCl. While the apparent rate of the fast-folding phase, λ_1 , continues to increase, the rate of the slower phase, λ_2 , decreases dramatically to produce a sharp downward inversion in the chevron. At 411 nm, however, refolding is monophasic at all concentrations of the denaturant. Also, within the limit of experimental error, the λ_1 measured at 430 nm and the single refolding rate measured at 411 nm both appear to have linear functional dependence on the denaturant concentration at all concentrations of GdnHCl, indicating apparent two-state kinetics of refolding.

The biphasic folding behavior and the downward inversion of λ_2 under strongly refolding conditions (≤ 1.5 M GdnHCl) is better illustrated by the fluorescence chevron shown in Figure 5(b). The unambiguously identifiable positive slope in the λ_2 versus GdnHCl concentration plot is shown in the inset to Figure 5(b). This behavior of λ_1 and λ_2 under native-like conditions indicates the existence of a folding (λ_1) as well as an unfolding (λ_2) reaction.

In examining the denaturant-dependence of λ_1 alone, we first consider the tests for two-state kinetics. The denaturant distribution of λ_1 measured by Soret absorbance at 430 nm along with the single rate observed at 411 nm indicates that the chevrons (Figure 5(a)) meet satisfactorily the criteria of two-state folding of ferrocyst *c*. The denaturant-dependence of λ_1 together with the single rate measured at 411 nm produce linear folding and unfolding limbs intersecting at ≈ 5 M GdnHCl. This feature simplifies the analysis of the rate-denaturant space. Values of $k_f(\text{H}_2\text{O})$ and $k_u(\text{H}_2\text{O})$, and $\Delta G(\text{H}_2\text{O})$ obtained from equations (4) are listed in Table 1. Considering the fast-folding molecules alone (λ_1 , 90%), these results indicate that, by the criterion of Soret heme absorbance, ferrocyst *c* folds-unfolds in a two-state manner.

In the case of the fluorescence chevron, however, the situation changes. The two-state folding criteria are satisfied only at higher concentrations of GdnHCl (≥ 3 M). Under native-like conditions, the folding limb of the λ_1 chevron rolls over. Similarly, the unfolding limb deviates away from linearity as the denaturant concentration in the unfolding medium is raised. These data do not fit equations (4). Although the rollover is generally taken to suggest accumulation of kinetic intermediates,³² we analyzed the λ_1 chevron according to equations (5) and (6), and compared the polynomial-fitted values of $k_f(\text{H}_2\text{O})$ and $k_u(\text{H}_2\text{O})$ with those expected for a two-state $N \leftrightarrow U$ transition. The value of $\Delta G(\text{H}_2\text{O})$ calculated in this way is ~ 4 -5 kcal mol⁻¹ higher than that determined from equilibrium unfolding data (Table 1, Figure 2). Given the noise in data and the long extrapolation of the unfolding limb to the ordinate, the significance of this disparity in the values of $\Delta G(\text{H}_2\text{O})$ is not clear.

Table 1. Kinetic parameters for folding and unfolding of ferrocyt *c* obtained by chevron analysis as described in the text

	$\log k_f(\text{H}_2\text{O})$		$\log k_u(\text{H}_2\text{O})$		$\Delta G(\text{H}_2\text{O})$ (kcal mol ⁻¹)			C_m M GdnHCl	
	Fitted ^a	Calculated ^b	Fitted ^a	Calculated ^b	From fits ^c	Calculated ^b	Equilibrium ^d	Kinetic ^e	Equilibrium ^d
Absorbance	3.3	-	-10.7 (-8.7) ^f	-	18.7 (16.05) ^f	-	18.8	~4.95	5.1
Fluorescence	2.7	2.1	-15.3 (-15.2) ^f	-16.7	23.2 (23.1) ^f	24.2	18.8	~4.95	5.1

^a By using equations (4) and (5) for absorbance and fluorescence data, respectively.

^b By using equation (6).

^c $-RT \ln[k_f(\text{H}_2\text{O})/k_u(\text{H}_2\text{O})]$.

^d Fit of data in Figure 2(d) by using equation (2), where $m_g \approx \Delta G(\text{H}_2\text{O})/C_m$.

^e Obtained from chevron.

^f Values obtained after correcting the observed unfolding rates according to $\log \lambda_{\text{corr}} = \log \lambda_{\text{obs}} + \log (\eta/\eta_0)$, where η and η_0 are viscosities in the presence and in the absence, respectively, of GdnHCl (see the text).

The chevron curvature indeed is poorly understood. A concentrated solution of GdnHCl is considerably viscous,³³ and this can contribute to the observed curvature in the chevron, especially in the unfolding limb.³⁴ To eliminate the effect of viscosity of the GdnHCl solution, we corrected the observed rates of unfolding by using the procedure suggested by Jacob & Schmid.³⁴ The corrected values are also plotted in Figure 5. The correction does alleviate the curvature in Figure 5(b), although not entirely. Values of $\log k_u(\text{H}_2\text{O})$ obtained now, using the same procedure as described above, are listed in Table 1. The value of $\Delta G(\text{H}_2\text{O})$ has decreased by 1.7 kcal mol⁻¹ in the case of heme absorbance-monitored folding, but has remained almost the same for fluorescence-monitored kinetics.

Signal amplitudes

Figure 6 shows quantitative analyses of the denaturant-dependence of Soret absorbance and fluorescence signal amplitudes at times $t=0$ and $t=\infty$ of folding and unfolding kinetics. The 411 nm and 430 nm absorbance at $t=0$ (S_0) of folding kinetics, normalized with reference to absorbance values of the unfolded protein, decreases as the GdnHCl concentration in the folding medium is lowered (Figure 6(a)). The area between the S_0 values and the unfolded baseline extrapolated linearly to native-like conditions contains the unobservable absorbance change associated with burst-phase folding kinetics. The GdnHCl-dependence of the S_0 values may be used to describe the equilibrium transition of the product of the burst phase reaction. There is some scatter in the S_0 values, and their GdnHCl dependence does not indicate a distinct denaturant-induced phase transition. The data have thus been fitted to the empirical relation:

$$S_0 = a + bx - cx(\exp(-dx))$$

where a , b , c and d are constants, and x is the concentration of GdnHCl. In unfolding kinetics, the S_0 values were comparable with the absorbance value of the native protein and, thus, the entire unfolding kinetic course is detected in the stopped-flow window.

Figure 6(b) shows the GdnHCl-dependence of S_0 and S_∞ fluorescence signals during folding and unfolding of the protein. All of what has been seen in the Soret absorbance-monitored kinetics (Figure 6(a)) is reproduced here. The fluorescence signal at $t=0$ of folding, S_0 , normalized with respect to the fluorescence of the initial unfolded protein, decreases as the GdnHCl concentration in the folding medium falls. Here again, there is some scatter in the S_0 values, and their denaturant-dependence has been fitted to

$$S_0 = a + bx - cx(\exp(-dx))$$

although the data can be force-fitted to describe a

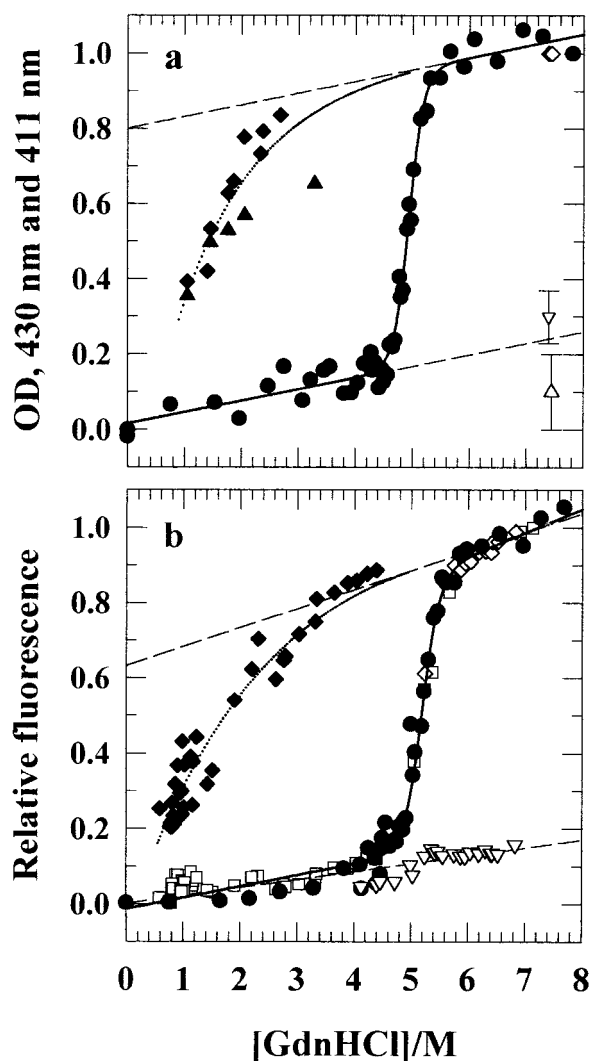


Figure 6. Normalized signal values at time $t=0$ and $t=\infty$ (S_0 and S_∞ , respectively) in folding and unfolding kinetics of reduced cyt *c* as a function of GdnHCl concentration. (a) Soret heme absorbance: S_0 from refolding monitored at 430 nm (\blacklozenge), and unfolding probed at 430 nm (∇) and 411 nm (\triangle). The continuous line through the equilibrium unfolding data is the same as described in Figure 2(a). (b) Tryptophan fluorescence: S_0 from refolding (\blacklozenge), and unfolding (∇), and S_∞ from refolding (\square) and unfolding (\diamond) experiments. The fluorescence-monitored equilibrium unfolding data (\bullet , see Figure 2(b)) are also plotted to show that kinetics were recorded for long enough for the protein to relax to equilibrium. The continuous line through the data has been drawn with $\Delta G(\text{H}_2\text{O}) = 19.4$ kcal mol⁻¹ and $m_g = 3.73$ kcal mol⁻¹ M⁻¹. Broken lines represent linear extrapolations of baselines. The area enclosed by S_0 values under the unfolded baseline extrapolated to the ordinate describes the unobservable amplitudes lost in the dead-time of stopped-flow. In the unfolding direction, the expected kinetic amplitude is accounted for almost entirely.

denaturant-induced cooperative melting of a structural species. In all unfolding kinetics no missing phase was detected, and as seen in Figure 6(b), the S_0 signal defines a simple linear extension of the native-state baseline to unfolding conditions, indicating the absence of any process faster than measurable by stopped-flow. Thus, no structural intermediate accumulates during unfolding of ferrocyst *c*. The $t = \infty$ signals in both folding and unfolding kinetic traces, S_∞ , reproduce the fluorescence values measured in the equilibrium unfolding experiment (Figure 2(b)), indicating that kinetics were recorded long enough for the protein to relax to equilibrium. The continuous line through the data has been drawn using equilibrium parameters for fluorescence given in the legend to Figure 2(b).

Independence of folding rates on protein concentration

To determine if higher protein concentration affects the observed rates, λ_1 and λ_2 , of ferrocyst *c* folding and, more importantly, to see if the slow phase consisting of 10–20% of the total observed amplitude, detectable only under strongly refolding conditions (≤ 1.5 M GdnHCl), is sensitive to protein concentration, refolding kinetics were recorded in which the protein concentration in the folding medium varied to a large extent but the final concentration of GdnHCl stayed the same. If the rate of the slow phase (λ_2) becomes slower with higher concentration of the protein, a possible structural attribute of the intermediate, whose accumulation produces the inversion in the folding chevron, could be a protein aggregate or a non-monomeric form. Figure 7(a) shows the two fluorescence-detected rates of refolding in the presence of 0.7 M GdnHCl as a function of protein concentration. In the concentration range 14–224 μ M, the observed rates are very similar. Also, the kinetics recorded by Soret heme absorbance, where refolding was allowed in the presence of ~ 0.7 M GdnHCl, yield rates that are not dependent on the concentration of the refolding protein (Figure 7(b)). The values of λ_1 measured at 430 nm and the single rate measured at 411 nm do show some scatter, but do not vary significantly with protein concentration. These results suggest that the slow refolding phase (λ_2) of ferrocyst *c* does not reflect aggregation-related kinetics.

Studies on pH-dependence of folding

Due to chain expansion in the unfolded state, the heme is likely to lose one or both of its native-state axial ligands, namely H18 and M80, the fifth and the sixth ligand, respectively. Indeed, it is well known that in the unfolded state of oxidized cyt *c*, the Fe^{3+} -M80 bond is broken, and the sixth axial site is occupied by non-native intrinsic polypeptide ligands, mainly H26 and H33, which interfere with correct chain folding.^{14,15} In the case of reduced cyt

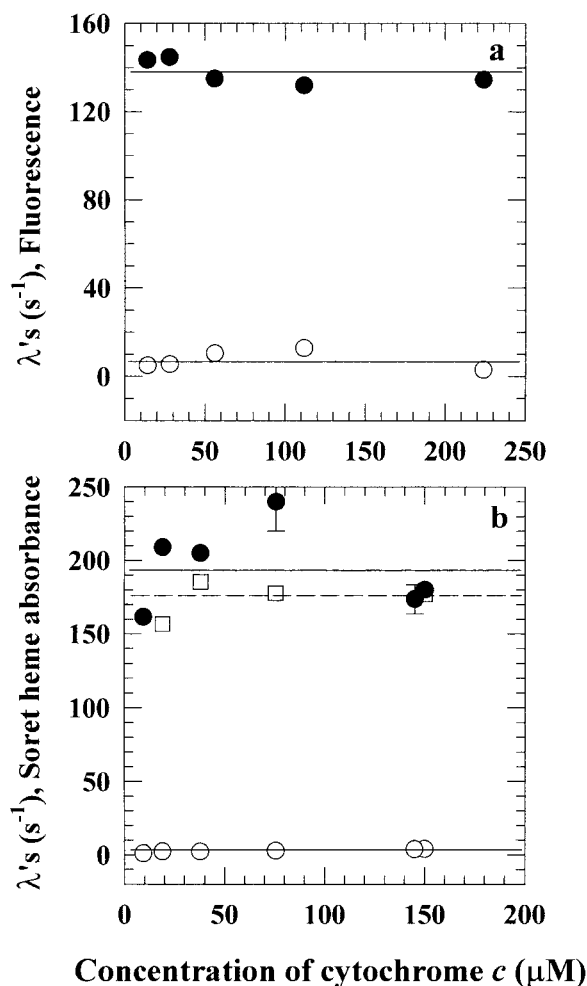


Figure 7. Protein concentration-dependence of observed rates of refolding in the presence of 0.7 M GdnHCl (neutral pH, 10 °C). (a) Tryptophan fluorescence: major phase (●), minor phase (○); (b) Soret absorbance: major (●) and minor (○) phases measured at 430 nm, and the single phase measured at 411 nm (□). Lines through data are approximations.

c also, the involvement of non-native heme ligands in giving rise to the slow phase of refolding (λ_2) is a possibility, although the chemistry of heme ligation in the unfolded state of ferrocyst *c* has not been worked out in detail. A standard test to detect the interference by non-native ionizable ligands during the refolding of cyt *c* is to vary the pH of the folding medium. Since the ligation of histidine residues to the heme iron is sensitive to the protonation state of the imidazole side-chain, changing the pH through the $\text{p}K_a$ region is expected to produce changes in the refolding kinetics in the case of interference by non-native heme ligation. To test if this is the case, we performed a set of equilibrium and stopped-flow experiments at different pH values.

The pH-dependent steady-state Soret spectra of unfolded ferrocytochrome *c*

Of the spectroscopic observables, Soret heme absorbance is particularly sensitive to pH-dependent heme ligation. Figure 8(a) shows a few Soret spectra of ferrocyt *c* unfolded in 7.3 M GdnHCl at the pH values indicated. Upon lowering the pH, the peak wavelength maximum, λ_{\max} , shifts slightly to the red. There are changes in intensity and bandshape also. As the pH is lowered, the intensity of the shoulder (~ 428 nm) observed in the neutral-pH spectrum (Figure 8(a); see also Figure 1(a)) grows, and the band broadens substantially to mask the shoulder. The bandshape and the λ_{\max} at low pH are very similar to those of

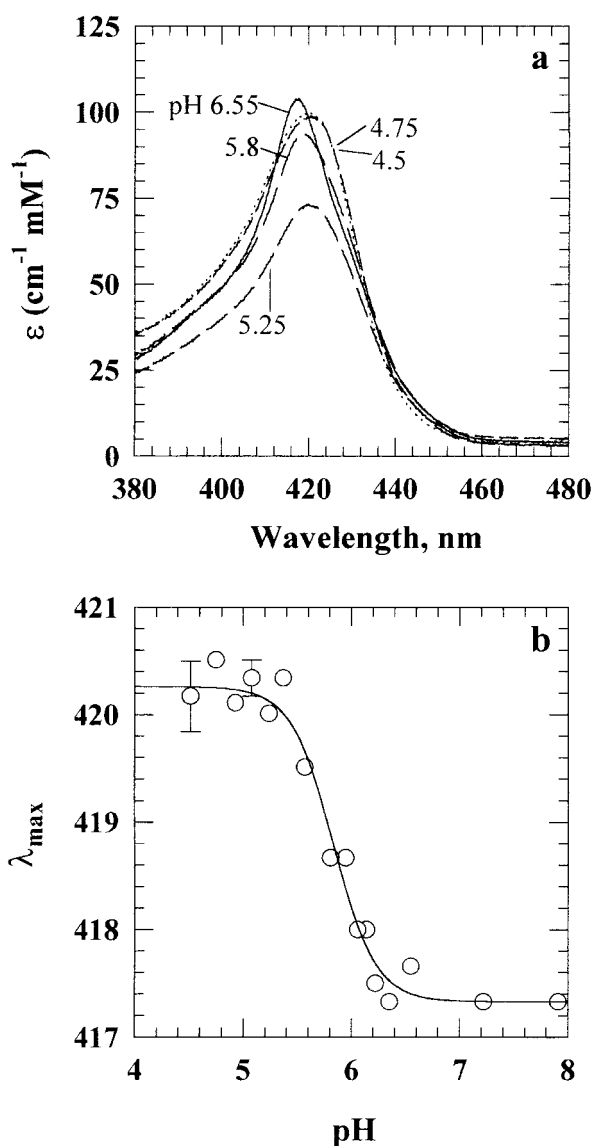


Figure 8. (a) pH-dependence of the Soret spectrum of ferrocyt *c* unfolded in 7.3 M GdnHCl (10 °C). (b) Shift of the Soret absorbance maximum, λ_{\max} , as a function of pH. The continuous line fit through the data (equation (3)) yields $pK_a = 5.85$ and $n = 2.2$.

deoxymyoglobin. Since the shoulder has been assigned, on the basis of the bandshape and the λ_{\max} , to a five-coordinate (high spin) ferrous iron complexed with H18 and the porphyrin,²² the results indicate an increase in the fraction of the equilibrium population of five-coordinate heme at low pH. But the low-pH band also shows substantial absorption at ~ 418 nm, indicating the persistence of a fraction of six-coordinate heme. This reshuffling of the equilibrium fractions of five and six-coordinate heme associated with the high pH to low pH transition is attributed to dissociation of potential non-native histidine ligands, consequent to protonation of the imidazole side-chain. The profile for the equilibrium proton titration of unfolded ferrocyt *c* is shown in Figure 8(b), where the value of λ_{\max} is plotted as a function of pH. The iterated fit parameters according to equation (3) yielded values of $pK_a = 5.85$ and $n = 2.2$. The pH titration of the unfolded protein was also measured by ^1H NMR (data not shown). The pH-dependence of unfolded-state chemical shifts of H26 C_2H (8.72 ppm) and H33 C_2H (8.69 ppm) yielded a higher value (~ 6.5) for the pK_a of both resonances. In any case, the value of pK_a within this range is characteristic of ionization of histidine side-chains, and the n value of 2.2 for the Soret absorbance data ($n = 1$ for each C_2H resonance in the NMR spectra) indicates the involvement of two coupled ionizations, implying heme ligation of both non-native histidine residues, H26 and H33, in the unfolded state of ferrocyt *c* at neutral pH.

What then constitutes the six-coordinate heme population at low pH? Cytochrome *c* has two methionine residues, M65 and M80, that can act as potential intramolecular heme ligands in the unfolded state. To check out the affinity of the methionine sulfur atom for the heme iron atom, we recorded Soret spectra of cyt *c* unfolded in 6.5 M GdnHCl in the presence of the model compound *N*-acetyl-DL-methionine (NAM). Figure 9(a) shows absolute absorption spectra of unfolded ferrocyt *c* in the presence of a 150-fold molar excess of NAM. The presence of NAM caused the shoulder collapse, indicating binding to the ferrous heme iron, so that all molecules become six-coordinate at equilibrium. It is interesting that under identical conditions unfolded ferrocyt *c* does not bind NAM (Figure 9(b)), consistent with the known poor affinity of methionine for the ferric heme iron.^{35–37} These observations indicate that at neutral pH a subfraction of the six-coordinate population of unfolded ferrocyt *c* is constituted of heme ligation of one or both methionine residues. Since the methionine sulfur atom is not expected to protonate in the pH range investigated here (pH 4.5–8), M65 and/or M80 ligate persistently to the heme iron of unfolded ferrocyt *c* constituting the six-coordinate heme population at low pH.

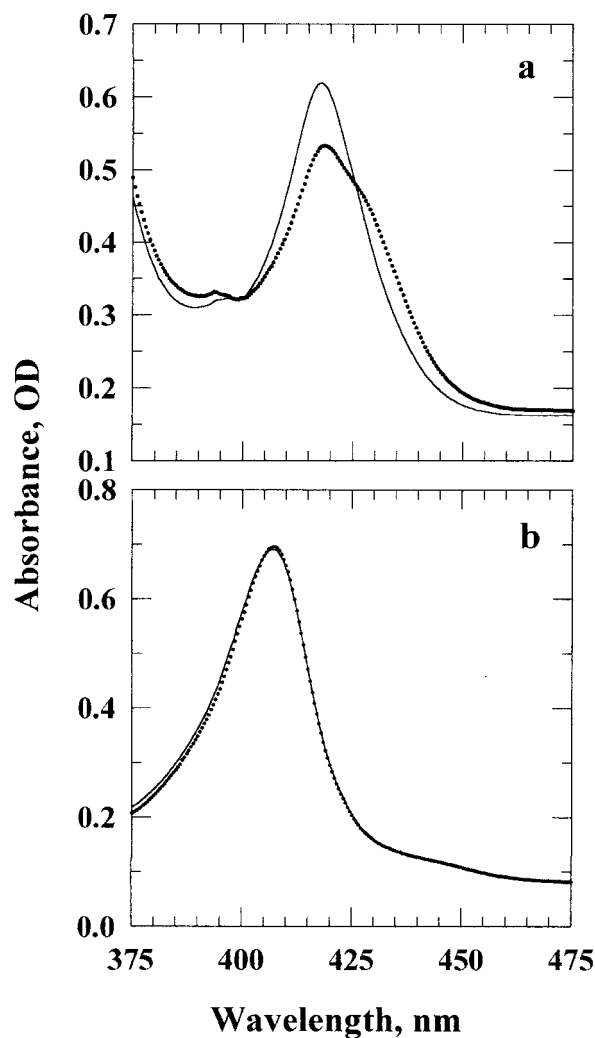


Figure 9. Soret region spectra of cyt *c* unfolded in 6.5 M GdnHCl (pH 6.9, 22°C), in the presence (—) and the absence (.....) of 150-fold excess of *N*-acetyl-DL methionine: (a) reduced cyt *c*; (b) oxidized cyt *c*.

The pH-dependent kinetics of refolding of ferrocyanochrome *c*

In this set of experiments, ferrocyanochrome *c*, unfolded in 7.5 M GdnHCl at neutral pH, was allowed to refold at different final pH values, but at a constant GdnHCl concentration of 1.25 M. Kinetics were monitored by Soret heme absorbance at 430 nm. Figure 10(a) shows that the two phases of refolding observed at neutral pH (see also Figures 3, 4, 5, and 7) appear also at low pH, and that the apparent rates of refolding are little affected by the pH of the refolding medium. The scatter in the rate of the fast phase is within error. The rates and the ~0.85:0.15 distribution of relative amplitudes of the major and the minor refolding phase are conserved in the pH range investigated (Figure 10(b)).

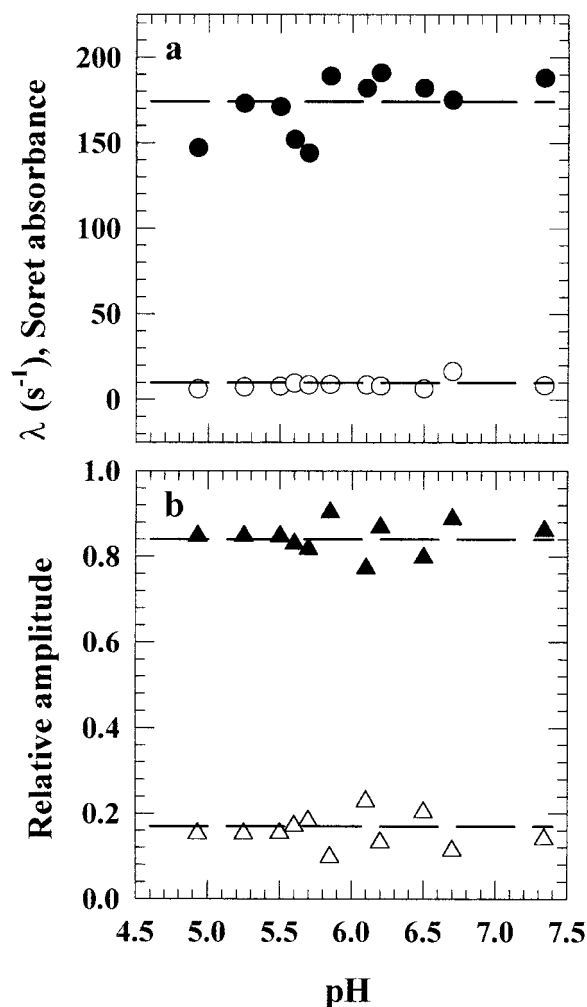


Figure 10. pH-dependence of observed (a) rates and (b) relative amplitudes of the two refolding phases measured by Soret absorbance at 430 nm. Filled and open symbols represent, respectively, rates or amplitudes of the major (λ_1) and the minor (λ_2) phase. The protein initially unfolded in 7.5 M GdnHCl (pH 7, 10°C), was allowed to refold in the presence of 1.25 M GdnHCl at different pH values.

The invariance of refolding rates at different final pH values is seen also when kinetics are monitored by tryptophan fluorescence (Figure 11). The relative amplitudes of the two refolding phases remain constant (not shown). In these experiments, the protein initially unfolded in 7 M GdnHCl at neutral pH was refolded in 1.4 M GdnHCl (variable pH).

The pH-dependent studies presented in this section provide two important results. (1) Types and the number of heme ligands in the unfolded state of ferrocyanochrome *c*. At neutral pH, with the sixth coordination site of the ferrous heme iron shared by H26, H33, M65, and M80, there is an equilibrium distribution of five and six-coordinate heme. The ionizations of the two histidine side-chains are

coupled, and at low pH they no longer serve as the heme ligand, so that the fraction of the neutral-pH five-coordinate heme increases. (2) The independence of folding kinetics on the heme ligation in the unfolded state. The kinetics of refolding of ferrocyanide *c* are not significantly different at neutral and low pH, indicating that heme ligation does not interfere with the refolding process. More importantly, the pH-independence of the apparent rate and the relative amplitude of the slow kinetic phase, which produces the chevron inversion under strongly native-like conditions (see Figures 5(a) and (b), and 10-12), indicates that the structural species associated with this kinetic phase is not related to heme misligation.

Kinetic modeling and calculation of microscopic rate constants

The observation of two phases of refolding under strongly native-like conditions by both fluorescence and heme absorbance necessitates the use of at least three species, N, U, and I, to describe the folding kinetics of ferrocyanide *c*. Denaturant distributions of the two observed rates, λ_1 and λ_2 , and equilibrium concentrations of the three species were simulated by numerical calculation of microscopic rate constants, k_j ($j = IU, UI, UN, \text{ and } NU$), within the formalism of linear rate-denaturant dependence (equation (8)). The procedure involved numerical calculation of the rate matrix by varying manually the microscopic rate constants in the absence of denaturant, $k_i(\text{H}_2\text{O})$, and the corresponding m_j^\ddagger values to obtain a denaturant distribution of λ_i and equilibrium concentrations of N, U, and I, that simulate the experimentally determined data. In this type of modeling, numeric instability is often encountered as a result of over-determination of some parameters. Satisfactory fits were obtained, however, by repetitive adjustment of parameters.

The three species, N, U, and I, can obviously yield the following three-state schemes.

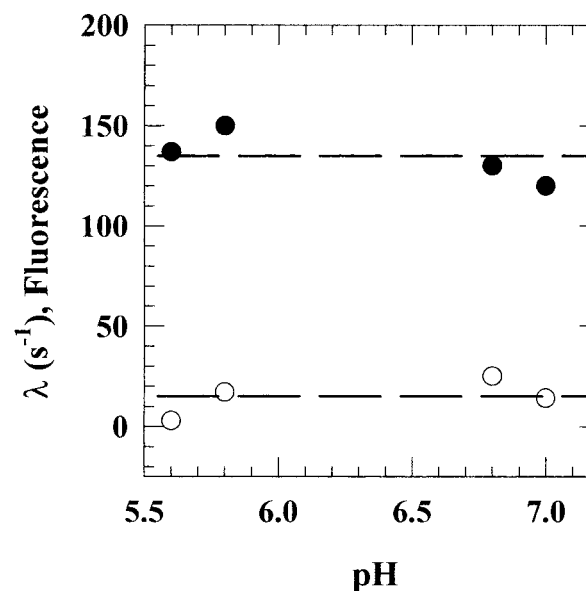
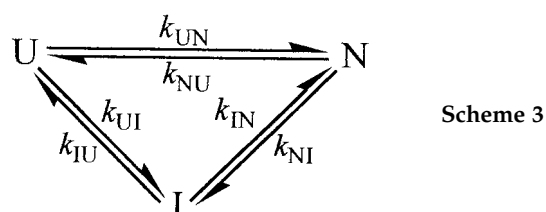
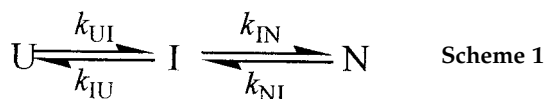


Figure 11. pH-dependence of refolding rates measured by fluorescence: the major phase (●), and the minor phase (○). In this case, the protein was unfolded in 7 M GdnHCl (pH 7), and was refolded in the presence of 1.4 M GdnHCl at different pH values.

All three schemes involve three species and two observable rate constants, λ_1 and λ_2 , so formal kinetic analysis cannot distinguish between the three mechanisms, even though six microscopic rate constants characterize the cyclic scheme as against four for any of the linear ones. The cyclic scheme has been used to describe a three-state model for lysozyme folding.³⁸ In the numerical analysis, the values for $k_i(\text{H}_2\text{O})$ and m_j^\ddagger can be adjusted such that any of the three mechanisms is able to fit correctly the observed denaturant dependence of λ_1 and λ_2 , and the equilibrium transition. A consideration of certain qualitative features of observed kinetics and chevrons (Figures 3-5), however, leads to rejection of Scheme 1. The inversion in the chevron of λ_2 that appears strikingly accentuated under strongly refolding conditions suggests that the intermediate has to unfold to the initial unfolded state in order to refold to N. Thus, I is not on the direct folding pathway, and Scheme 1 may be dropped. Both Schemes 2 and 3 can describe the chevron. Since there is no experimental evidence for conversion of I to N directly during folding, Scheme 2 is preferred to Scheme 3. In fact, Scheme 3 effectively reduces to Scheme 2 as k_{IN} and k_{NI} become vanishingly small.

On the basis of these considerations, Scheme 2 has been used to describe a classical mechanism of folding of ferrocyanide *c*. Each of the two data sets, Soret heme absorbance and fluorescence, was simulated individually. The values of kinetic and thermodynamic parameters derived from one of the solutions of eigenvalue simulation for each

data set are listed in Table 2. The denaturant-dependences of λ_i and microscopic rate constants, k_{IU} , k_{UI} , k_{UN} , and k_{NU} , are shown in Figure 12. The calculated rate spaces for the two chevrons are nearly identical (Figure 12(b) and (d), and Table 2). The differences in values of $k_{UN}(\text{H}_2\text{O})$ and $k_{IU}(\text{H}_2\text{O})$ between the two data sets are within experimental error.

Discussion

Two-state equilibrium transition of ferrocycytochrome *c*

Observation of a highly cooperative phase transition using a single spectroscopic probe in an equilibrium unfolding experiment in bulk sample of a protein does not often provide sufficient ground to conclude that the protein undergoes a two-state transition. To establish the existence of only two equilibrium states, N and U, the unfolding data must fit the equation of a two-state model of protein unfolding, and transitions recorded by a wide variety of probes, providing information at different structural level of the protein, must be superimposable. The available data for the three

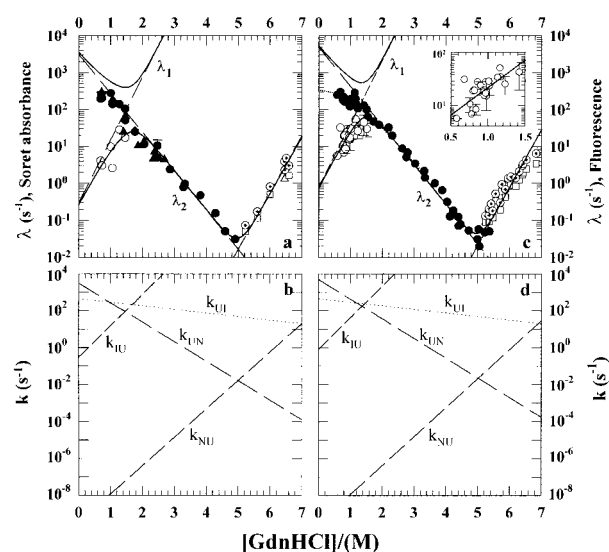


Figure 12. Results of numerical calculation of eigenvalues (λ_1 and λ_2) and microscopic rate constants (k_i) for the $I \leftrightarrow U \leftrightarrow N$ mechanism. (a) Eigenvalue simulation of the folding chevron measured by Soret absorbance. (b) The k_i -denaturant space derived from simulation of data in (a). (c) Eigenvalue simulation of the fluorescence-measured folding chevron. The inset shows the inverted dependence of λ_2 on GdnHCl concentrations less than ~ 1.5 M, suggesting the unfolding of I to U. The dotted line through λ_1 (●) has been drawn to guide the eye through a small degree of rollover in the folding arm of the chevron. (d) The k_i -denaturant space for the three-state model simulation of fluorescence-measured data. The thermodynamic parameters obtained from model simulation are listed in Table 2. Note that the identity of symbols in this Figure is same as in Figure 5.

probes employed (Figure 2) suggest that the equilibrium unfolding of ferrocycytochrome *c* involves only the native and the unfolded state without accumulation of structural intermediates to any detectable level. This conclusion is reached only within the limit and the resolution of equilibrium unfolding experiments. There are perhaps several short-lived partially unfolded forms of ferrocycytochrome *c*, and at least one of these states is identifiable by stopped-flow NMR hydrogen exchange measurements under moderate to strongly destabilizing conditions.²³

Stability of ferrocycytochrome *c*

Equilibrium stability of proteins (i.e. the difference in Gibbs free energies of native and unfolded states) fall in the 5-20 kcal mol⁻¹ range.^{39,40} A linearly extrapolated $\Delta G(\text{H}_2\text{O})$ value of $18.8(\pm 1.45)$ kcal mol⁻¹, and a C_m value of $5.1(\pm 0.15)$ M GdnHCl at 10°C indicate that reduced cyt *c* is one of the most stable proteins known to date. This value of $\Delta G(\text{H}_2\text{O})$ agrees well with the native-state hydrogen exchange-measured stability of 17.8 kcal mol⁻¹ at 30°C.⁴¹ In the oxidized state, the same protein unfolds reversibly, registering a $\Delta G(\text{H}_2\text{O})$ value of $9.1(\pm 1.2)$ kcal mol⁻¹ (e.g. see Tsong³⁰). Given that the crystal structures of cyt *c* in the two oxidation states do not show any significant oxidation state-dependent polypeptide positional shifts,⁴²⁻⁴⁴ the conformational origin of a large difference in free-energy of unfolding, $\Delta\Delta G(\text{H}_2\text{O}) \sim 11$ kcal mol⁻¹, is intriguing, although in the case of yeast iso-1-cyt *c*, the stabilization ($\Delta\Delta G(\text{H}_2\text{O}) \approx 6$ kcal mol⁻¹) has been suggested to be entirely entropic.⁴⁵ Oxidation state-dependent structural changes are found only in relation with heme structural adjustments and movement of internally bound water molecules,⁴⁴ suggesting two possible sources of extra-stabilization of ferrocycytochrome *c*. (1) At neutral pH, the oxidized heme has a +1 charge because of the unpaired electron of the ferric iron atom (low spin). The burial of a +1 charge, as in the case of oxidized cyt *c*, alters the heme solvation, and consequently is destabilizing.⁴⁶ Upon reduction, the net charge on the heme iron is reduced to zero, which is energetically preferred in the low dielectric of the protein interior. (2) The reduced heme iron has the intrinsic ability to delocalize its electrons into the orbitals of the sulfur atom. The increased overlap between the low-lying empty 3d orbitals of sulfur provided by the side-chain of M80 and the 3d orbitals of Fe²⁺ (the so-called d-d overlap) results in an outstanding stability of the Fe²⁺—M80 bond in reduced cyt *c*,⁴⁴ thus strengthening the heme-polypeptide interaction. The bond is so strong that even CO fails to break it in the native state of the molecule.⁴⁷ In contrast, the Fe³⁺—M80 bond is very weak in oxidized cyt *c*, and extrinsic ligands such as imidazole and cyanide can replace the M80 ligand even in the native state. In fact, as discussed below, the affinity of the reduced heme iron atom for the sulfur atom of M80, and the Fe²⁺—M80 bond

Table 2. Kinetic parameters for the I \leftrightarrow U \leftrightarrow N model for folding and unfolding of ferrocyst *c* at 10 °C, neutral pH

Probe	$k_{UN}(\text{H}_2\text{O})$	m_{UN}^\ddagger	$k_{NU}(\text{H}_2\text{O})$	m_{NU}^\ddagger	$k_{IU}(\text{H}_2\text{O})$	m_{IU}^\ddagger	$k_{UI}(\text{H}_2\text{O})$	m_{UI}^\ddagger	ΔG_{IU}^a	ΔG_{UN}^a	C_m^a
Fluorescence	5.0×10^3	-1.38	3.0×10^{-10}	2.05	0.8	2.22	450	-0.25	3.55	17.04	5.02
Absorbance	3.1×10^3	-1.36	3.5×10^{-10}	1.98	0.3	2.20	450	-0.25	4.10	16.70	5.01

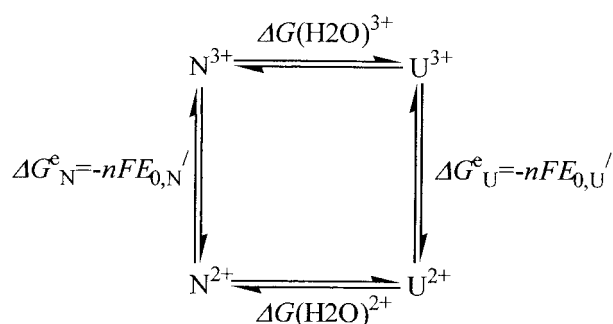
Values of microscopic rate constants in the absence of denaturant, $k_i(\text{H}_2\text{O})$, and the m_i^\ddagger values are given in s^{-1} and $\text{kcal mol}^{-1} \text{M}^{-1}$, respectively.

^a Apparent equilibrium free energies (kcal mol^{-1}), and transition midpoints (C_m) obtained from three-state model calculations.

strength would appear to contribute to the speed of folding of ferrocyst *c* relative to that of ferricyt *c*.

Linkage between conformational stability and redox potential of cytochrome *c*

The Gibbs free-energy change for electrochemical reduction is given by $\Delta G^e = -nFE_0'$, where n is the number of electrons added during reduction, F is the Faraday constant (23.06 kcal mol⁻¹ V⁻¹), and E_0' is the redox potential of cyt *c*. For native horse cyt *c* at neutral pH, an $E_{0,N}'$ of 254 mV⁴⁸ translates to the standard free energy change of reduction of -5.9 kcal mol⁻¹. On this basis, the higher conformational stability of reduced cyt *c* was rationalized long ago.⁴⁹ Experimentally, the thermodynamic stability of each redox state can be individually estimated from equilibrium unfolding transitions, and the $\Delta G(\text{H}_2\text{O})$ values for the two redox states can be related to the E_0' values of the native and the unfolded couple as:



where: $\Delta G(\text{H}_2\text{O})^{2+}$, the free energy of unfolding of ferrocyst *c*, is ~ 18.8 kcal mol⁻¹ (Figure 2(d)); $\Delta G(\text{H}_2\text{O})^{3+}$, the free energy of unfolding of ferricyt *c* is $9.1(\pm 1.2)$ kcal mol⁻¹ (see Tsong³⁰); and $\Delta G_N^e = -nFE_{0,N}'$, the Gibbs free energy of electrochemical reduction of native cyt *c*, is -5.9 kcal mol⁻¹. Since in the thermodynamic cycle $\Sigma \Delta G_j^i = 0$, the value of $\Delta G_U^e = -nFE_{0,U}'$, the free energy difference of oxidized and reduced cyt *c* in their unfolded states, is 3.8 kcal mol⁻¹. Thus, $E_{0,U}' = -164$ mV.

The value of $E_{0,U}'$ calculated in this work compares fairly well with the value of $-200(\pm 25)$ mV,⁵⁰ and -167 mV,²¹ both determined in previous electrochemical studies on GdnHCl-unfolded cyt *c*. These values of $E_{0,U}'$ are, however, in poor agreement with redox potentials of naked heme. For example, in the presence of NAM, the heme-containing octapeptide of horse cyt *c* (residues 18-26) that lacks the polypeptide tertiary fold, shows an E_0' of -45 mV,³⁶ indicating a role of the unfolded polypeptide in determining the electrochemical properties of the heme in unfolded cyt *c*.

The expense of negative redox potential of unfolded cytochrome *c*

The greater the absolute value of E_0' , the further apart are free energies of the redox couple. A drastic fall in the redox potential of cyt *c* (from 254 mV to -164 mV) accompanying protein unfolding reduces the ground-state free energy difference between the two oxidation states. Consequently, the reduced heme iron becomes extremely susceptible to oxidation by molecular oxygen dissolved in the solution, making experimental studies of ferrocyst *c* folding very difficult. Extreme care must be taken to exclude oxygen from protein solutions. Working in an inert atmosphere with freshly prepared, degassed solutions containing a slight excess of sodium dithionite yields satisfactory and reproducible results.

Fast refolding of ferrocystochrome *c*

Some 80-90% of ferrocyst *c* molecules fold extremely fast. The fastest observable rate, λ_1 , measured in this study is 295 s⁻¹ in the presence of 0.7 M GdnHCl at 10 °C. We could not measure refolding at a still lower concentrations of GdnHCl because of several technical reasons and experimental difficulties. In the absence of chevron rollover, and when the folding-unfolding reaction is two-state, it is possible to evaluate the true rate of refolding in the absence of denaturant, $k_{UN}(\text{H}_2\text{O})$, by linearly extrapolating λ_1 from the middle of the chevron to the ordinate. The λ_1 chevron shows rollover when measured by fluorescence, but is linear when measured by heme Soret absorbance (Figure 5(a) and (b)). Soret absorbance data have been fitted to a two-state U \leftrightarrow N transition (Figure 5(a)) that yields a good estimate of $k_u(\text{H}_2\text{O}) = 2000$ s⁻¹ ($\tau = 500$ μ s; see Table 1). Numerical simulations to fit the Soret absorbance data to I \leftrightarrow U \leftrightarrow N (Scheme 2) yields a slightly higher value ($k_{UN}(\text{H}_2\text{O}) = 3100$ s⁻¹, $\tau = 322$ μ s; see Figure 12(a) and (b), and Table 2). Similar results have been obtained from fluorescence data (Figure 12(c) and (d), and Table 2). These values, estimated from 10 °C data, appear consistent with the estimate of ~ 130 μ s at 40 °C reported by Pascher *et al.*,²⁶ who took advantage of the stability difference of the two oxidation states of cyt *c* (see above) and initiated refolding of reduced cyt *c* to a narrow range of final GdnHCl concentration by using an optical trigger method that rapidly injects an electron into the ferric heme of unfolded oxidized cyt *c*.

The fast-folding molecules of ferrocystochrome *c* display two-state kinetics

The two-state nature of folding and unfolding kinetics of a homogeneous protein population is established when the following conditions are satisfied. (1) Both folding and unfolding kinetics are monophasic. Measurements using fluorescence and

Soret heme absorbance (430 nm) show that ~80-90% of molecules of ferrocyst *c* fold fast in a single observable kinetic phase in the range of pH and protein concentrations investigated. Also, unfolding of the native protein is monophasic.

(2) The linearity of chevron plots. The logarithm of λ_1 values are dependent linearly on GdnHCl concentration when measured by Soret absorbance at both 411 and 430 nm (Figure 5(a)), but are not when measured by tryptophan fluorescence (Figure 5(b)). Although the deviation from linearity is taken as an indication of accumulation of kinetic intermediates,³² the curvature in chevron plots is not always a disqualification for two-state kinetics of a protein. For example, the unfolding limb of the fluorescence chevron of ferrocyst *c* shows a curvature (Figure 5(b)) even though amplitude analysis of the time traces of unfolding kinetics (Figures 4(c) and 6(b)) shows the absence of burst kinetics, and hence two-state unfolding. It is also known that chevron plots may be curved for two-state proteins when the transition state moves along the top of a broad activation energy barrier.^{51,52} Polynomial analysis of the fluorescence λ_1 chevron (Figure 5(b)) for two-state criterion (equations (5) and (6)),⁵¹ however, yielded a refolding rate constant slightly different from that calculated from $\log K$ and $\log k_u(\text{H}_2\text{O})$ (Table 1). The lack of close correspondence of values may be largely due to substantial uncertainty in the value of $\log k_u(\text{H}_2\text{O})$ obtained by long extrapolation of the unfolding limb to the ordinate by applying the quadratic relationship between $\log k_u$ and GdnHCl concentration (equations (5)). The assumption of the quadratic relationship has no theoretical basis. The use of equations (5) is based on empirical observation of the curvature of the unfolding limb, and it is uncertain if the curvature extends below the transition region. Another basic question remains: why is the λ_1 chevron curved in fluorescence-measured kinetics, but linear in the heme Soret-monitored kinetics (Figure 5)? Clearly, more work will be needed in this direction.

(3) Consistency in values of protein stability parameters, $\Delta G(\text{H}_2\text{O})$, C_m , and m , determined from the folding chevron and from two-state analysis of equilibrium unfolding transitions. The values of these parameters calculated from analyses of λ_1 chevrons measured by fluorescence and heme optical absorption, and from two-state analysis of the equilibrium unfolding data are compared in Table 1. The correspondence is seen best for the heme absorbance data. This result is expected if the fast-folding molecules of ferrocyst *c* are kinetically two-state.

Slow refolding of ferrocystochrome *c*: existence of a dead-end kinetic intermediate

Under native-like conditions, a slow phase (λ_2) of folding of ferrocyst *c* is detected. This phase must

exist under all folding conditions, but is not detectable in the deeper regions of the chevron, since any kinetic species involved is destabilized at higher concentrations of denaturant. When the folding milieu is made more stabilizing by lowering the final concentration of the denaturant, the kinetic intermediate accumulates, and hence the slow folding phase appears. While the observed rate of this kinetic phase, λ_2 , becomes progressively slower as more native-like conditions are approached (Figures 5(a) and (b), and 12), its amplitude is a constant at 10-20% (Figures 3(b) and 4(b)). From these two observations, it is concluded that upon initiation of refolding, 10-20% of ferrocyst *c* chains are misfolded to an intermediate conformational state in which the protein segments cannot be reconfigured correctly to yield the native conformation. The unproductive misconfigured structure must then unfold to the initial state for correct refolding. The minimal representation of this observation is $I \leftrightarrow U \leftrightarrow N$, where *I* is the dead-end intermediate.

We have no information about the rate of formation of *I*. It is likely that it is formed in the sub-millisecond regime or, setting a lower limit, during the fast phase of the observable kinetics. What is measured in the slow kinetic phase is the rate of unfolding of *I* to *U* (i.e. λ_2). As soon as $I \rightarrow U$ conversion occurs, the *U* molecules enter the fast folding channel. Thus, for these 10-20% molecules, the $I \rightarrow U$ process sets the rate of refolding.

Possible structural properties of the dead-end intermediate

The observation that refolding kinetics of ferrocyst *c* are independent of both protein concentration (Figure 7) and pH (Figures 10 and 11) suggest that the dead-end intermediate detected in our experiments is not a protein aggregate, unlike those described for proteins U1A and CI2.⁵³ The structure of the intermediate is unknown. Nonetheless, the available data help portray a possible structural picture of the intermediate. An interesting feature of the profile of denaturant-dependence of λ_2 (Figures 5(a) and (b), and 12(a) and (c)) is the sizeable positive slope. The kinetic m value for the unfolding of *I*, m_{IU}^\ddagger , is 2.2 for both fluorescence and Soret absorbance data (Figure 12 and Table 2). The value of m_{IU}^\ddagger is large and comparable with the value of m_{NU}^\ddagger , suggesting an extraordinary large-scale burial of surface area in the intermediate.

What indications do the observable spectroscopic properties provide about the structural nature of *I*? Because of the close proximity of W59 and the heme group in native cyt *c*, Förster energy transfer makes the molecule fluorescence-silent. Since structural unfolding of cyt *c*, resulting in an increase in W59-heme distance, is accompanied by an increase in fluorescence, the slow unfolding of *I* to *U* might also be expected to produce a kinetic phase of increasing fluorescence. The observation

presented is, however, to the contrary: the $I \rightarrow U$ reaction does not produce an increase in fluorescence, nor does the heme absorbance at 430 nm increase, indicating apparently that in *I*, as in *U*, the heme is not within the quenching proximity of W59, and that the symmetry and ligation properties of the heme, which cause change in Soret absorbance properties between *N* and *U* states, are very similar in *U* and *I*. There is, however, a caveat in this argument. Any change in spectroscopic properties for the $I \rightarrow U$ reaction will be detectable only if *U* populates significantly on the $I \rightarrow U \rightarrow N$ pathway. Given that the $U \rightarrow N$ reaction is rapid ($\lambda_1 > \lambda_2$), this is not expected to occur.

Its off-pathway nature makes clear that the intermediate has misconfigured chain segment(s). For *cyt c*, a strong candidate responsible for misfold chain organization is the non-native histidine-heme ligation in the unfolded state. It has been known for the oxidized form of *cyt c* that persistent non-native histidine-heme ligation in the unfolded state causes the histidine residues (H26 and H33) to be trapped in the protein interior during folding, and consequently, the H26 and H33-resident portions of the polypeptide are misplaced. As discussed in detail in the following section, such non-native histidine-heme ligation does not interfere with the refolding of reduced *cyt c*. Further, the off-pathway intermediate of ferrocyanide *c* is observed even under conditions where any possible non-native histidine-heme ligation is blocked by lowering the pH of the refolding medium (Figures 8, 10 and 11). The constant amplitude of λ_2 observed at different pH values (Figure 10) suggests that formation and accumulation of *I* is not dependent on the refolding of the five-coordinate heme population. Thus, it appears that the misfolded organization of chain segments in *I* may occur as a result of random non-specific hydrophobic collapse leading to mass burial of non-polar groups.

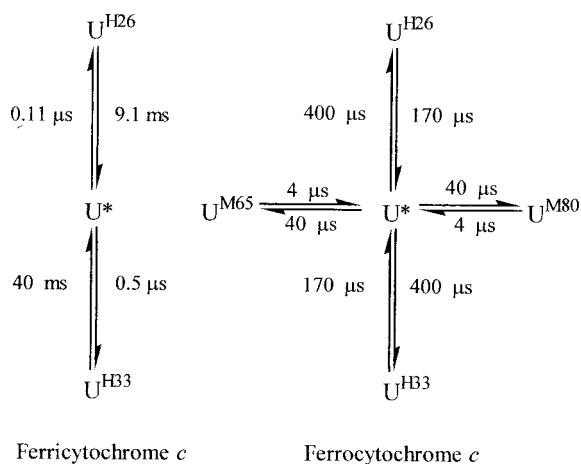
Non-interference by heme ligation with the folding reaction of ferrocyanide *c*

Even though oxidized *cyt c* has served as a prototype in protein folding studies ever since the early studies by Tanford and co-workers,^{4,7} its importance appears marred because of unwanted non-native heme ligation in the unfolded state that complicates folding.^{14–16} In view of this fact, and to discuss the present results in perspective, it is imperative to examine how heme ligation would affect the folding of reduced *cyt c*, having established that the reduced protein is energetically more stable than the oxidized one by ~ 10 kcal mol⁻¹. Here, we produce a model of heme-ligation intrachain dynamics to trace the origin of kinetic misfolding, and to demonstrate how the folding of ferrocyanide *c* is indifferent to ligand-based complications.

The model

In native *cyt c*, H18 and M80 serve as the fifth and the sixth coordination ligand, respectively, of the heme iron. Upon unfolding at neutral pH, the iron—H18 bond stays intact, but the iron—M80 bond is ruptured in both ferricyanide *c*^{15,54–56} and ferrocyanide *c* (A.K.B., unpublished results). While H18 persists as the fifth coordination ligand in both oxidation states at all pH values except under strongly acidic conditions, the sixth coordination site becomes available for potential intrachain heme ligands, namely H26, H33, M65, and M80²² (A.K.B., unpublished results). Equilibrium occupancy of these ligands would depend on their binding affinity to the iron atom in a given oxidation state. Unfolded molecules of ferricyanide *c* contain H26 and H33 as the sixth coordination ligand;^{15,55,57} the possible coordination of M65 or M80 is excluded because of poor affinity of the oxidized heme iron atom for sulfur-based ligands (Figure 9(b); see also Berghuis & Brayer⁴⁴). In fact, the affinity of the oxidized heme iron for the methionine sulfur atom is so poor that the Fe³⁺—M80 bond is ruptured even on mild alkalization of a solution of native ferricyanide *c*.⁵⁸ On the other hand, the ferrous heme iron atom preserves its affinity for methionine ligands even when ferrocyanide *c* is unfolded. Thus, all four intrachain ligands can serve as the sixth coordination ligand of the heme iron of ferrocyanide *c* in the form of transient contacts.

Now, the equilibrium occupancy of these ligands at the sixth coordination site of the heme iron atom, and hence the equilibrium fraction of five and six-coordinate heme populations in a given oxidation state of *cyt c* can be estimated from data on transient binding and dissociation of heme ligands at the sixth coordination site. The dissociation time constants for H26 and H33 in unfolded ferricyanide *c*, measured in a previous study by rapidly lowering the pH of the unfolded protein solution, are 9.1 ms and 40 ms, respectively.¹⁵ The corresponding time constants for association, estimated from the equilibrium constant for imidazole binding to a ferricyanide *c* peptide, which is 8318 M⁻¹ (see Harbury & Loach⁵⁹), are 110 ns and 500 ns, respectively. The ligand exchange rates at the heme site of unfolded ferrocyanide *c* have been determined from nanosecond laser photolysis of a carbon monoxide complex.^{22,24} Photodissociation of the carbon monoxide ligand opens up the heme site to binding by intrachain heme ligands, resulting in a competition between intramolecular ligand binding and CO rebinding. By fitting this model to transient spectral data following CO photolysis, the binding and dissociation time constants were found to be 40 μ s and 4 μ s, respectively, for the methionine residues M65 and M80, and 400 μ s and 170 μ s, respectively, for the histidine residues, H26 and H33. These processes and the time constants for both oxidation states of *cyt c* are summarized in the following scheme for heme-ligand interactions in the unfolded state.



Here, U^* represents the five-coordinate form, and subscripts to U indicate ligands bound to the heme iron atom. By using these time constants, the equilibrium fraction of U^* can be calculated from the following conditions:

$$U^* + U^{H26} + U^{H33} = 1$$

$$U^* + U^{H26} + U^{H33} + U^{M65} + U^{M80} = 1$$

The values obtained for U^* are 0.6×10^{-5} and 0.45 for ferricyt *c* and ferrocycytochrome *c*, respectively. These values suggest that virtually all unfolded molecules of ferricyt *c* have six-coordinate heme moieties carrying non-native histidine ligands, whereas only ~55% ferrocycytochrome *c* molecules have six-coordinate heme moieties bonded to all four intrapolyptide ligands.

Ferrocycytochrome c folds slower than ligand dissociation

How do these equilibria affect the folding reaction of cyt *c*? In the case of ferrocycytochrome *c*, 45% of the unfolded molecules, which have no equilibrium occupancy at the sixth coordination site of the heme, will fold unaffected. For the remaining 55%, a liganded form will enter the folding pathway only if the rate of dissociation of the ligand from the heme iron atom is slower than the folding rate (see Zwanzig⁶⁰). The dissociation time constants for all four ligands of ferrocycytochrome *c* are smaller than the refolding time constant of $\sim 370(\pm 180)$ μ s found in this study. Of course, the native M80 ligand will offer its side-chain sulfur atom for ferrous iron bonding, possibly very early during folding. Thus, heme-ligation in the unfolded state of ferrocycytochrome *c* does not interfere with refolding.

Ferricytochrome c folds faster than ligand dissociation

On the other hand, at neutral pH all unfolded molecules of ferricyt *c* enter the folding pathway with non-native histidine residues bonded to the

ferric heme iron, and the dissociation times of these histidine residues are larger by at least two orders of magnitude than the fastest folding time constant of ~ 50 μ s measured in microsecond capillary mixing experiments.^{19,61} As a result, during refolding of ferricyt *c*, the histidine residues, along with the polypeptide segments that they belong to, become trapped in the folding structure. There have been several discussions about the role of histidine trapping in ferricyt *c* folding.^{14,15,57} Whatever the role, the act of displacing the histidine resident chain segments from the distal side of the heme moiety to the proximal side of M80 slows folding at later stages. The misconfigured chain organization must spend a long time in a frozen state before the dissociation of non-native histidine residues yields to complete folding.

Merits of the model

The model predicts that ligand trapping and associated complications will affect only the late events of folding and not the fast events. Indeed, in the case of ferricyt *c*, the early events (τ in μ s) are independent of heme ligation state, but late events (τ in 100 ms range) are ligation-dependent.¹⁹ For example, when ligation of non-native histidine residues is blocked by carrying out experiments in the presence of imidazole, the fast events persist but the intermediate phase is suppressed completely.¹⁹ Imidazole is an extrinsic ligand and does not allow chain misconfiguration. In this study of ferrocycytochrome *c*, we do not observe variation of folding kinetics with pH ranging from neutral to approaching less than 5, because the ligand dissociation is inherently faster, and does not allow misfolded organization of the polypeptide.

Kinetic partitioning during refolding of ferrocycytochrome *c*

We need to know where the two phases of refolding of ferrocycytochrome *c* originate from. Two sources can give rise to distinct kinetic phases of refolding: conformationally heterogeneous populations of unfolded molecules, and partitioning of a homogeneous unfolded population very early during folding. Kinetic partitioning may also occur within a set of structurally homogeneous molecules in a heterogeneous unfolded population, amplifying the number of refolding phases. Both population heterogeneity and kinetic partitioning could potentially account for the fact that the relative amplitudes of the fast and the slow phase are constants (0.8-0.9 and 0.1-0.2, respectively) as a function of GdnHCl concentration.

Heterogeneity in the unfolded population of yeast iso-2-cyt *c*, arising from coupling of pH-dependent histidine protonation to histidine-heme misligation and proline isomerization, has been reported recently.⁶² The unfolded population of horse cyt *c* is, however, not known to be heterogeneous, except that, as indicated in earlier double

jump experiments by Ridge *et al.*,¹⁰ a minor, proline-related, slow-folding species exists in ferricyt *c*. More recent studies suggest that the proline-related, slow-folding species account for only ~5% of unfolded molecules.^{15,63} In the case of ferrocyt *c* also, the existence of a slow-folding population of unfolded ferrocyt *c* is not precluded. Two results, (i) the rate of the slow phase is much higher than the proline isomerization-limited folding rate, 0.1–0.01 s⁻¹ typically, and (ii) the rates show very strong dependence on GdnHCl concentration, strongly indicate that proline-related population heterogeneity is not involved. Another possible source of population heterogeneity in cyt *c* is based on heme ligation. But, as discussed above, perturbation of heme ligation does not affect the refolding kinetics of ferrocyt *c*. Further, the equilibration amongst various liganded forms is so fast that different liganded populations are irresolvable in the folding time-scale. There could still be other sources of heterogeneity of unfolded ferrocyt *c* that we are not aware of, but the unfolded-state NMR spectra under a variety of different conditions have thus far not indicated any (A.K.B., unpublished results).

Thus, the available indications point to kinetic partitioning as the mechanism of segregation of unfolded ferrocyt *c* very early during refolding. While 80–90% of molecules enter a direct folding channel, the remaining 10–20% enters an unproductive channel to arrive at a dead-end.

Burst phase kinetics of ferrocyclochrome *c* folding

Observation of the earliest structure formation during protein folding is often limited by the time window provided by conventional stopped-flow instruments. With an instrument dead-time of ~1.5–2 ms, as experimentally determined, microsecond folding events are obviously not observed. The general procedure, when direct microsecond measurements are not done, is to quantify the stopped-flow burst phase signal as a function of denaturant concentration and then subject the data to meaningful interpretations. Unfortunately, this procedure suffers from practical limitations of obtaining relatively accurate burst phase data (at the fastest measured rate of 295 s⁻¹, as reported here, even 1 ms discrepancy in the determination of the mixing dead-time will affect the measured burst phase amplitude drastically), and from the viewpoint of interpretation. Burst phase signals may often arise from submillisecond non-specific structural rearrangements or simply contraction of the unfolded polypeptide in response to its transfer from the unfolding solvent to a strongly refolding solvent, as is done in a stopped-flow experiment. That such is indeed the case, has been shown for refolding of RNase A and ferricyt *c*.^{64,65} In the case of ferricyt *c*, a recent submillisecond study has shown that very little secondary structure is formed in the submillisecond burst phase.⁶⁶ Ultra-

fast CD measurements of reduced cyt *c* folding triggered by electron transfer have shown that very little secondary structure is formed in the sub-millisecond time-domain.⁶⁷

The burst phase data for ferrocyt *c* (Figure 6) are even harder to interpret, for one thing: the signals are convoluted by processes from both U → N and U → I pathways. The problem would have been alleviated if we were able to measure the rate of U → I directly. Considering the two-state nature of the U → N reaction, as suggested by analyses of λ₁ chevrons monitored by Soret heme absorbance at 411 and 430 nm, and by fluorescence (Figure 5(a) and (b), and Table 1), the folding burst signals may appear to arise from fast events in the U → I pathway leading to the formation of one or more early kinetic intermediate. This interpretation, which rests on the assumption that U → I is not a two-state reaction, is incompatible with the observation that only 10–20% of molecules enter the U → I pathway, whereas almost the entire expected signal amplitude is lost in the dead-time under strongly native-like conditions. Thus, the burst phase probably represents non-specific events faster than the observed rates. The non-specific events could be, as suggested by others,⁶⁸ ultrafast solvent reorganization coupled to chain contraction in response to transfer of the unfolded polypeptide from strongly unfolding to strongly refolding conditions. The GdnHCl-dependence of the burst signal appears monotonous, and the noise in the data (Figure 6) does not permit a functional description of the signal on the denaturant. It may be noted that in the three-state (I ↔ U ↔ N) model calculations, we have not invoked the occurrence or the nature of the burst reaction. Clearly, more studies will be needed to understand what happens during the folding burst phase of ferrocyt *c*.

Absence of kinetic unfolding intermediate

In contrast with folding kinetics, the kinetics of unfolding of ferrocyt *c* are slow and simple. All spectroscopic probes used in this study have indicated the absence of burst unfolding reactions (Figure 6 (a) and (b)), suggesting that no kinetic intermediate is involved during unfolding. In an earlier study, we had reported burst unfolding reactions during unfolding of oxidized cyt *c*, measured by tryptophan fluorescence and far-UV CD.⁶⁹ Several later repeats of CD kinetics, however, revealed that there actually was no burst unfolding phase of dissolution of secondary structure, and the earlier CD results were incorrect due to instrumental error (unpublished results; T. Sosnick, personal communication).

The mechanism of folding of ferrocyclochrome *c*

The two major findings of this study are the fast direct folding of 80–90% of unfolded molecules (τ ~ 370(±180) μs, estimated from kinetic modeling and chevron fits) with no apparent accumulation

of kinetic folding intermediates, and the slow folding of the remaining 10-20% of unfolded molecules that first fold to an off-pathway intermediate, I, that can fold to the native state only by first unfolding back to the U state such that the rate of $I \rightarrow U$ conversion sets the limit of folding of I to N. Important control experiments have suggested that I is not a protein aggregate, nor is it an artifact of heme misligation. The results of analyses in this study do not appear to indicate involvement of any other kinetic species in the refolding of ferrocyst *c*.

The apparent lack of kinetic intermediates in the refolding of 80-90% of unfolded molecules of ferrocyst *c* needs some discussion in the light of available hydrogen exchange (HX) results. In the first HX experiment on ferrocyst *c* in subdenaturing to strongly denaturing conditions by the use of real-time NMR methods,²³ we have reported the accumulation of a partly unfolded structure of ferrocyst *c* similar to a ferricyt *c* kinetic folding intermediate in which the N and C-terminal helices dock in an orthogonal fashion.^{12,15} Native-state HX studies by Xu *et al.*⁴¹ later identified two more such structures, and they suggest that these three partially unfolded forms compose a refolding-unfolding pathway common to both the oxidized and the reduced form of cyt *c*. Although the validity of assignment of partially unfolded forms, detected by equilibrium measurements of HX, to kinetic intermediates has been questioned,^{70,71} at least one intermediate, that detected by us²³ and by Xu *et al.*,⁴¹ has been described in HX labeling and proton NMR studies on ferricyt *c*.¹² This folding intermediate in which only the terminal helices of cyt *c* are folded (the partially unfolded form labeled rygB by Englander and co-workers⁴¹) must be very short-lived. It accumulates to a detectable level in the folding of ferricyt *c*, because its lifetime is prolonged by chain misconfiguration consequent upon non-native heme ligation (Sosnick *et al.*, 1994, Elove *et al.*, 1994), but escapes detection in the folding of ferrocyst *c* because of non-interference of heme ligands with the folding. Our models presented here illustrate this point clearly.

Other results of this study, especially the burst phase signals, can be interpreted somewhat inconclusively to include one or more early structural intermediates, but we have not invoked their existence in the description of the minimal mechanism for folding involving only I, U, and N (Scheme 2). The proposed $I \leftrightarrow U \leftrightarrow N$ model is based primarily on the experimental observation of a fundamental kinetic criterion for the accumulation of an off-pathway intermediate; namely, an inversion of the GdnHCl-dependence of one of the observed rate constants for folding, λ_2 . This direct observation obviates the need for checking out the other off-pathway kinetic criteria based on ϕ value analysis,⁷² pulse-chase competition experiments,⁷³ and the evaluation by experiments of various microscopic rate constants as suggested by Bai.⁷⁴ The numerical simulation of the data to this model,

which predicts the microscopic rate constants and the thermodynamic parameters characterizing the stability of the protein in a consistent manner, lends additional support to the validity of this minimal mechanism. It is, of course, obvious that in higher concentrations of denaturant (>1.5 M GdnHCl), where I does not accumulate because $k_{IU} \gg k_{UV}$, the $I \leftrightarrow U \leftrightarrow N$ mechanism reduces to the simple $U \leftrightarrow N$ mechanism. We do not have structural data at molecular or atomic resolution, and the mechanism presented here is based on a phenomenological kinetics model. It is emphasized that the $I \leftrightarrow U \leftrightarrow N$ scheme is the simplest and the minimal model to interpret the available data. The actual mechanism could be more complex. For a detailed view of structural and energetic considerations further studies using high-resolution techniques will be needed to dissect the folding process.

Implications of an off-pathway intermediate

In the realm of classical models of folding, we operationally define an off-pathway intermediate as one that has to undergo, because of its arrival at the dead-end, a large-scale unfolding to resemble the initial unfolded state both structurally and energetically. Observation of a large m^\ddagger value for the $I \rightarrow U$ step in the ferrocyst *c* folding (Figures 5 and 12, and Table 2) illustrates this point. An on-pathway intermediate, on the other hand, does not have to unfold structurally except for occasional rupture of a few long-range interactions or rearrangement of folding chain segments such that it can continue to fold to the native state. Both off and on-pathway intermediates can result from initial chain collapse and formation of local interactions such that both states are lower in energy relative to the unfolded state, and both of them would appear to reduce the conformational search problem. Many proteins fold by engaging one or more kinetic intermediates,^{1,2} and structural properties of a sizeable number of protein intermediates have been characterized at atomic level. While the question of which of these intermediates are on-pathway and which are off can be investigated further by recently described methods,^{73,74} the on-pathway situation would appear more encouraging, because such intermediates are expected to speed folding by guiding the folding chain to the native state. Structural and kinetic characterization of these intermediates can help elucidate the folding process.

On the other hand, when off-pathway, as defined here to suit the classical folding model, the role of kinetic intermediates becomes less obvious. It would appear that the formation of the off-pathway intermediate is a natural consequence of kinetic partitioning at the incipient phase of folding.

A discussion of an off-pathway role of intermediates from the standpoint of theoretical models is not straightforward, for these models refrain from using on-pathway and off-pathway terminol-

ogies. According to numerical results from Monte Carlo simulations of protein-like polymers on a lattice,^{75–80} and molecular dynamics simulation of heteropolymers in continuum,^{81,82} a heteropolymer/protein quickly acquires a compact structure carrying native as well as non-native contacts. During further evolution, some native-like structural elements are dissolved, while others are formed. That such is the case has been suggested for folding of β -lactoglobulin, for which a non-native α -helical conformation formed during the burst folding is transformed to the native β -sheet conformation.⁸³ Dill & Chan⁵ call this intermediate off-pathway, because it does not increasingly resemble the native state while on the folding run. A similar scenario might explain the recently discovered transient formation and disappearance of non-native β -sheet during folding of α -lactalbumin.⁸⁴ Secondary structural dissolution, as has been shown for plastocyanin,⁸⁰ may occur when a neighboring structural element fails to find conformations consistent with the native state. Folding is thus not unidirectional and may involve minima in which parts of the polypeptide exist misconfigured. The system explores more stable minima corresponding to denser packing with increasing number of native-like contacts on a longer time-scale. Folding can be slow also when, for example, interactions among non-polar groups become very strong. Such hydrophobic patches force the polypeptide to become stuck in local minima of wrong compact conformations.

Materials and Methods

A commercial preparation of horse cyt *c* (type VI from Sigma) was used without further purification. GdnHCl and sodium dithionite was obtained from Gibco BRL and Aldrich, respectively. Other chemicals were reagent grade. Concentrations of GdnHCl in solutions were determined by refractive index measurement⁸⁵ using an Abbe type refractometer (Milton Roy). Unless stated otherwise, all experiments were done in 0.1 M sodium phosphate buffer at 10 °C. All solutions were stored and handled in an inert atmosphere. To avoid vapor condensation on the outer surface of cuvettes, a constant stream of nitrogen was used during all equilibrium and kinetic measurements. Extreme care was taken to minimize air exposure of solutions at all stages of the experiments.

Equilibrium unfolding measurements

Cytochrome *c* solutions, prepared in the 0–8 M GdnHCl range contained 8 μ M, 10 μ M, and 12.6 μ M, protein for Soret optical absorption, fluorescence, and far-UV CD measurements, respectively. Solutions were reduced under nitrogen with 0.5–2 mM sodium dithionite and incubated at 10 °C in tightly capped quartz cuvettes for 45 minutes. Absorbance values at 411 nm and 430 nm, which are positive and negative λ_{max} , respectively, in the Soret region of the difference spectrum of native and unfolded ferrocyt *c*, were read from spectra recorded in the 375–600 nm range using a Cary 100 (Varian) spectrophotometer. Tryptophan fluorescence excited at 280 nm (slit-width 0.75 nm) was measured at

358 nm (slit-width 1.25 nm) using a 1 cm square cuvette in a photon-counting instrument (SPEX 320). Far-UV CD was measured at 222 nm using a 1 mm cuvette. All CD measurements were done using a JASCO J720 spectropolarimeter.

pH titration of the unfolded protein

The pH of a solution of 7.3 M GdnHCl, buffered in 50 mM sodium phosphate, 50 mM sodium acetate, was adjusted to different values in the range 7.9–4.5. Addition of acid or base for adjusting pH values caused little change in denaturant concentration. A few microliters of a concentrated solution of cyt *c* was added to these denaturant solutions such that the final protein concentration was 4 μ M. The samples in the oxidized state were incubated at room temperature for an hour. They were transferred to 1 cm square cuvettes, reduced with \sim 500 μ M sodium dithionite under a constant stream of nitrogen, and equilibrated for about five minutes. Soret spectra (480–380 nm) were recorded at room temperature using a Cary 100 spectrophotometer.

Measurement of folding-unfolding kinetics

For refolding, cyt *c* (0.09 mM, and 0.4 mM for Soret heme absorbance, and fluorescence, respectively) was initially unfolded in \sim 7.5 M GdnHCl, 0.1 M phosphate (pH 7), and equilibrated at room temperature overnight. The protein solution was cooled to 10 °C, reduced by the addition of 5 mM sodium dithionite, and equilibrated at the same temperature for \sim 15 minutes under argon. Two buffers, one containing \sim 8 M GdnHCl and another with no GdnHCl, both at neutral pH, were reduced by the addition of \sim 0.5–1 mM sodium dithionite shortly before the experiment. The protein and buffer solutions were filled in gas-tight syringes and loaded into the stopped-flow mixing module, which was exhaustively washed with deionized water containing 5 mM sodium dithionite. Folding to different final concentrations of GdnHCl was initiated by mixing 33 μ l of the unfolded protein solution with 267 μ l of the two buffers mixed variably. In experiments where kinetics were studied under strongly refolding conditions, 25 μ l of the protein solution was mixed with 275 μ l of the refolding buffer, so that the final concentration of GdnHCl could be minimized. The final concentrations of folding proteins were 7.5–9 μ M and 33–40 μ M in Soret absorbance and fluorescence-monitored kinetics, respectively. After recording kinetics, the waste solutions were collected to check the GdnHCl concentrations to which the protein refolded, and to record visible absorption spectra to ensure that the protein had stayed reduced during the course of measurements. To minimize oxidation of reduced cyt *c* and to avoid degradation of sodium dithionite, the unfolded protein solution and the buffers were reduced in batches. Each batch of freshly reduced solutions provided \sim 20–30 shots. Unfolding experiments were performed following the same procedure. For unfolding, the native protein solution was prepared in \sim 1 M GdnHCl.

An SFM3 mixing module (Biologic) regulated at 10 °C by the use of an external water-bath was employed for kinetic measurements. For fluorescence measurement, 280 nm excitation source was obtained from a 150 W xenon lamp. Emission by the mixed solution contained in a 1.5 mm square flow-cell was measured using a 320 nm cutoff filter. Data were acquired using the soft-

were provided by Biologic. Typically, 10-20 shots were averaged for noise reduction.

At later stages of this study, an SFM4 instrument was used to repeat several experiments that were done earlier with the SFM3 instrument. The major advantage of using the SFM4 instrument was acquisition of higher precision fluorescence and heme optical absorbance data at sufficiently lower concentration of denaturant. A 0.8 mm square flow-cell was used. The dead-time, determined experimentally by using the procedure suggested by the instrument manufacturer, was ~1.5-2 ms.

Analysis of equilibrium unfolding curves

Raw data plotted as absorbance, fluorescence and CD signals as a function of GdnHCl were least-squares fitted to a two-state $N \leftrightarrow U$ model using equation (1):⁸⁶

$$S_{\text{obs}} = \frac{C_f + m_f[D] + C_u + m_u[D] \exp\left(\frac{-\Delta G + m_g[D]}{RT}\right)}{1 + \exp\left(\frac{-\Delta G + m_g[D]}{RT}\right)} \quad (1)$$

where S_{obs} is the observed signal, C_f and C_u , and m_f and m_u represent intercepts and slopes of native and unfolded baselines, respectively. m_g (or the equilibrium m value), is a parameter related to the change in surface area during the global unfolding of the protein, and D represents the concentration of GdnHCl. The far-UV CD signals in the native-state baseline region were fitted to $C_f + m_f[D] + m_{f2}[D]^2$

For a close comparison of Soret absorbance, fluorescence, and CD-monitored unfolding of ferrocyst *c*, the data sets were individually normalized, and converted to plots of fraction unfolded as a function of GdnHCl concentration. The resultant data sets were fitted according to:

$$\begin{aligned} -RT \ln K &= -RT \ln K(\text{H}_2\text{O}) - m_g[\text{GdnHCl}] \\ &= m_g(C_m - [\text{GdnHCl}]) \end{aligned} \quad (2)$$

where K is the equilibrium constant (ratio of the fraction denatured to the fraction native), and C_m is the transition midpoint.

Analysis of pH titration data

The peak wavelength of Soret spectra (λ_{max}) as a function of pH was fitted to the equation:

$$\lambda_{\text{max}} = A + \frac{\Delta\lambda_{\text{max}}}{\{1 + 10^{n(\text{pH} - \text{pK}_a)}\}} \quad (3)$$

where, A is the value of λ_{max} (=417.3) at pH 7.9, $\Delta\lambda_{\text{max}}$ is the total change in peak wavelength in going from pH 7.9 to pH 4.5, n is the number of protons titrated, and pK_a is the apparent pK of the titration.

Analysis of kinetic traces

Kinetic traces were fitted to single or double-exponential functions to obtain apparent rates, λ_i , the initial signal, S_0 , which corresponds to the zero-time signal in the stopped-flow window, the observed signal, S_{obs} , and the final equilibrium signal, S_{∞} . The S_0 , S_{obs} , and S_{∞} signals were subjected to initial normalization by first subtracting the buffer signals, and then dividing by the recorded signal of the unfolded protein in the highest GdnHCl

concentration. At this stage, GdnHCl-dependence of S_0 and S_{∞} signals describe the titration of the missing amplitude, which is lost within the dead-time of measurement, and the equilibrium global transition, respectively. To obtain the total expected signal (unfolded minus folded) in a given GdnHCl concentration, the pre and post-transition baselines were linearly extrapolated to abscissa values of 8 M and 0 M, respectively. If S_N and S_U represent the baseline-extrapolated signal values of the native and the unfolded protein in a given denaturant concentration, the missing fraction of the signal can be calculated by $(S_{N(U)} - S_0) / (S_{N(U)} - S_{U(N)})$.

Chevron analysis

The λ_1 dependence on GdnHCl concentration measured by Soret heme absorbance was analyzed according to the two-state model, $N \leftrightarrow U$:

$$K = \frac{[U]}{[N]} = \frac{k_u}{k_f}$$

$$\lambda_1 = k_u + k_f \quad (4)$$

$$\log k_u = \log k_u(\text{H}_2\text{O}) + m_u[\text{GdnHCl}]$$

$$\log k_f = \log k_f(\text{H}_2\text{O}) + m_f[\text{GdnHCl}]$$

where, $k_u(\text{H}_2\text{O})$ and $k_f(\text{H}_2\text{O})$ are unfolding and refolding rate constants, respectively, in the absence of GdnHCl.

Denaturant-dependences of λ_1 measured by fluorescence were analyzed by polynomial fits.⁵¹

$$\log k_f = \log k_f(\text{H}_2\text{O}) + m_{1,f}[\text{GdnHCl}] - m_{2,f}[\text{GdnHCl}]^2$$

$$\log k_u = \log k_u(\text{H}_2\text{O}) + m_{1,u}[\text{GdnHCl}] - m_{2,u}[\text{GdnHCl}]^2 \quad (5)$$

The fitted values of $k_f(\text{H}_2\text{O})$ and $k_u(\text{H}_2\text{O})$ along with the corresponding m values were compared with those calculated by the use of the equations:

$$\begin{aligned} \log k_f(\text{H}_2\text{O}) &= \log k_u(\text{H}_2\text{O}) - \log K(\text{H}_2\text{O}) \\ \log k_u(\text{H}_2\text{O}) &= \log k_f(\text{H}_2\text{O}) + \log K(\text{H}_2\text{O}) \end{aligned} \quad (6)$$

where:

$$\log K(\text{H}_2\text{O}) = -\Delta G(\text{H}_2\text{O}) + \frac{m_g[\text{GdnHCl}]}{2.3RT}$$

Simulation of kinetic data

To interpret the observed folding kinetics of reduced cyt *c*, the following minimal scheme was used:



For numerical calculation of the microscopic rate constants, k_j ($j = IU, UI, UN, \text{ and } NU$), a 3×3 rate matrix was set up from the three coupled linear differential equations for I , U , and N . The eigenvalues, λ_i ($i = 1, 2$), computed by diagonalizing the rate matrix are functions of k_j s, the logarithm of which are assumed to have linear dependence on GdnHCl concentration.^{87,88}

$$\ln k_j = \ln k_j(\text{H}_2\text{O}) + \frac{m_j^*[\text{GdnHCl}]}{RT} \quad (8)$$

where $k_j(\text{H}_2\text{O})$ is the value of k_j in the absence of GdnHCl and m_j^* is related to the change in surface area. The apparent kinetic rates (i.e. stopped-flow observables) were thus simulated with calculated λ_i values by adjusting the $k_j(\text{H}_2\text{O})$ and m_j^* values as input parameters. The equilibrium unfolding transitions were calculated from the eigenvectors by assigning expected values of absorbance and fluorescence to I, U, and N in the range 0 to 1.

Acknowledgements

This work was supported by the School of Chemistry, University of Hyderabad (AKB), and by a research grant from the Department of Biotechnology, Government of India (JBU). A few preliminary NMR experiments were carried out in the NMR facility at CIL, University of Hyderabad, and in the National Facility for High Resolution NMR, TIFR, Bombay.

References

1. Matthews, C. R. (1993). Pathways of protein folding. *Annu. Rev. Biochem.* **62**, 653-683.
2. Roder, H. & Colón, W. (1997). Kinetic role of early intermediates in protein folding. *Curr. Opin. Struct. Biol.* **7**, 15-28.
3. Schindler, T., Herrler, M., Marahiel, M. A. & Schmid, F. X. (1995). Extremely rapid protein folding in the absence of intermediates. *Nature Struct. Biol.* **2**, 663-673.
4. Ikai, A. & Tanford, C. (1971). Kinetic evidence for incorrectly folded intermediate states in the refolding of denatured proteins. *Nature*, **230**, 100-102.
5. Dill, K. A. & Chan, H. S. (1997). From Levinthal to pathways to funnels. *Nature Struct. Biol.* **4**, 10-19.
6. Stellwagen, E. (1968). The reversible unfolding of horse heart ferricytochrome *c*. *Biochemistry*, **7**, 2893-2898.
7. Ikai, A., Fish, W. W. & Tanford, C. (1973). Kinetics of unfolding and refolding of proteins II. Results for cytochrome *c*. *J. Mol. Biol.* **73**, 165-184.
8. Knapp, J. A. & Pace, C. N. (1974). Guanidine hydrochloride and acid denaturation of horse, cow, and *Candida krusei* cytochrome *c*. *Biochemistry*, **13**, 1289-1294.
9. Tsong, T. Y. (1976). Ferricyt *c* chain folding measured by the energy transfer of tryptophan 59 to the heme group. *Biochemistry*, **15**, 5467-5473.
10. Ridge, J. A., Baldwin, R. L. & Labhardt, A. M. (1981). Nature of the fast and slow refolding reactions of iron (III) cytochrome *c*. *Biochemistry*, **20**, 1622-1630.
11. Myer, Y. P. (1984). Ferricytochrome *c*. Refolding and the methionine 80-sulfur-iron linkage. *J. Biol. Chem.* **259**, 6127-6133.
12. Roder, H., Elöve, G. A. & Englander, S. W. (1988). Structural characterization of folding intermediates in cytochrome *c* by H-exchange labelling and proton NMR. *Nature*, **335**, 700-704.
13. Jeng, M. F. & Englander, S. W. (1991). Stable submolecular folding units in a non-compact form of cytochrome *c*. *J. Mol. Biol.* **221**, 1045-1061.
14. Sosnick, T. R., Mayne, L., Hiller, R. & Englander, S. W. (1994). The barriers in protein folding. *Nature Struct. Biol.* **1**, 149-156.
15. Elöve, G. A., Bhuyan, A. K. & Roder, H. (1994). Kinetic mechanism of cytochrome *c* folding: involvement of the heme and its ligands. *Biochemistry*, **33**, 6925-6935.
16. Sosnick, T. R., Mayne, L. & Englander, S. W. (1996). Molecular collapse: the rate limiting step in two-state cytochrome *c* folding. *Proteins: Struct. Funct. Genet.* **24**, 413-426.
17. Takahashi, S., Yeh, S-R., Das, T. K., Chan, C-K., Gottfried, D. S. & Rousseau, D. L. (1997). Folding of cytochrome *c* initiated by submillisecond mixing. *Nature Struct. Biol.* **4**, 44-50.
18. Chan, C-K., Hu, Y., Takahashi, S., Rousseau, D. L., Eaton, W. A. & Hofrichter, J. (1997). Submillisecond protein folding kinetics studied by ultrarapid mixing. *Proc. Natl Acad. Sci. USA*, **94**, 1779-1784.
19. Shastry, M. C. R. & Roder, H. (1998). Evidence for barrier-limited protein folding kinetics on the microsecond time scale. *Nature Struct. Biol.* **5**, 385-392.
20. Bhuyan, A. K., Elöve, G. A. & Roder, H. (1991). Redox effects on protein stability and folding kinetics of horse cytochrome *c*. *J. Cell. Biochem.* **15G**, 188.
21. Bixler, J., Bakker, G. & McLendon, G. (1992). Electrochemical probes of protein folding. *J. Am. Chem. Soc.* **114**, 6938-6939.
22. Jones, C. M., Henry, E. R., Hu, Y., Chan, C. K., Luck, S., Bhuyan, A. *et al.* (1993). Fast events in protein folding initiated by nanosecond laser photolysis. *Proc. Natl Acad. Sci. USA*, **90**, 11860-11864.
23. Bhuyan, A. K. & Udgaonkar, J. B. (1998). Stopped-flow NMR measurement of hydrogen exchange rates in reduced horse cytochrome *c* under strongly destabilizing conditions. *Proteins: Struct. Funct. Genet.* **32**, 241-247.
24. Goldbeck, R. A., Thomas, Y. G., Chen, E., Esquerra, R. M. & Kliger, D. S. (1999). Multiple pathways on a protein-folding energy landscape: kinetic evidence. *Proc. Natl Acad. Sci. USA*, **96**, 2782-2787.
25. Luck, S. D., Bhuyan, A. K. & Roder, H. (1992). Folding Fe(II)-CO cytochrome *c* by photolysis. *Biophys. J.* **64**, A173.
26. Pascher, T., Chesick, J. P., Winkler, J. R. & Gray, H. B. (1996). Protein folding triggered by electron transfer. *Science*, **271**, 1558-1560.
27. Eaton, W. A. & Hofrichter, J. (1981). Polarized absorption and linear dichroism spectroscopy of hemoglobin. *Methods Enzymol.* **76**, 175-261.
28. Bushnell, G. W., Louie, G. V. & Brayer, G. D. (1990). High-resolution three dimensional structure of horse heart cytochrome *c*. *J. Mol. Biol.* **214**, 585-595.
29. Vanderkooi, J. M. & Erecinska, M. (1975). Cytochrome *c* interaction with membranes. Absorption and emission spectra and binding characteristics of iron-free cytochrome *c*. *Eur. J. Biochem.* **60**, 199-210.
30. Tsong, T. Y. (1974). The Trp-59 fluorescence of ferricytochrome *c* as a sensitive measure of the over-all protein conformation. *J. Biol. Chem.* **249**, 1988-1990.
31. Brems, D. N. & Stellwagen, E. (1983). Manipulation of the observed kinetic phases in the refolding of denatured ferricytochromes *c*. *J. Biol. Chem.* **258**, 3655-3660.
32. Matouschek, A., Kellis, J. T., Jr, Serrano, L., Bycroft, M. & Fersht, A. R. (1990). Transient folding intermediates characterized by protein engineering. *Nature*, **346**, 440-445.

33. Kawahara, K. & Tanford, C. (1966). Viscosity and density of aqueous solutions of urea and guanidine hydrochloride. *J. Biol. Chem.* **241**, 3228-3232.
34. Jacob, M. & Schmid, F. X. (1999). Protein folding as a diffusional process. *Biochemistry*, **38**, 13773-13779.
35. George, P. & Schejter, A. (1964). The reactivity of ferrocyanide with iron-binding ligands. *J. Biol. Chem.* **239**, 1504-1508.
36. Harbury, H. A., Cronin, J. R., Fanger, M. W., Hettlinger, T. P., Murphy, A. J., Myer, Y. P. & Vinogradov, S. N. (1965). Complex formation between methionine and a heme peptide from cytochrome *c*. *Proc. Natl Acad. Sci. USA*, **54**, 1568-1664.
37. Schejter, A. & Aviram, I. (1969). The reaction of cytochrome *c* with imidazole. *Biochemistry*, **8**, 149-153.
38. Wildegger, G. & Kiefhaber, T. (1997). Three-state model for lysozyme folding: triangular folding mechanism with an energetically trapped intermediate. *J. Mol. Biol.* **270**, 294-304.
39. Privalov, P. L. (1979). Stability of proteins: small globular proteins. *Advan. Protein Chem.* **33**, 167-241.
40. Dill, K. A. (1990). Dominant forces in protein folding. *Biochemistry*, **29**, 7133-7155.
41. Xu, Y., Mayne, L. C. & Englander, S. W. (1998). Evidence for an unfolding and refolding pathway in cytochrome *c*. *Nature Struct. Biol.* **5**, 774-778.
42. Takano, T. & Dickerson, R. E. (1981a). Conformation change of cytochrome *c*. I. Ferrocyanide structure refined at 1.5 Å resolution. *J. Mol. Biol.* **153**, 79-94.
43. Takano, T. & Dickerson, R. E. (1981b). Conformation change of cytochrome *c*. II. Ferricyanide refinement at 1.8 Å and comparison with the ferrocyanide structure. *J. Mol. Biol.* **153**, 95-115.
44. Berghuis, A. M. & Brayer, G. D. (1992). Oxidation state-dependent conformational changes in cytochrome *c*. *J. Mol. Biol.* **223**, 959-976.
45. Cohen, D. S. & Pielak, G. J. (1995). Entropic stabilization of cytochrome *c* upon reduction. *J. Am. Chem. Soc.* **117**, 1675-1677.
46. Churg, A. K. & Warshel, A. (1986). Control of the redox potential of cytochrome *c* and microscopic dielectric effects in proteins. *Biochemistry*, **25**, 1675-1681.
47. Schejter, A. & Plotkin, B. (1988). The binding characteristics of the cytochrome *c* iron. *Biochem. J.* **255**, 353-356.
48. Loach, P. A. (1976). Oxidation-reduction potentials, absorbance bands and molar absorbance of compounds used in biochemical studies. In *Handbook of Biochemistry and Molecular Biology* (Fasman, G. D., ed.), 3rd edit., vol. 1, pp. 123-130, CRC Press Inc., Cleveland, OH.
49. Margoliash, E. & Schejter, A. (1966). Cytochrome *c*. *Advan. Protein Chem.* **21**, 113-286.
50. Ferri, T., Poscia, A., Ascoli, F. & Santucci, R. (1996). Direct electrochemical evidence for an equilibrium intermediate in the guanidine-induced unfolding of cytochrome *c*. *Biochim. Biophys. Acta*, **1298**, 102-108.
51. Silow, M. & Oliveberg, M. (1997). High-energy channeling in protein folding. *Biochemistry*, **36**, 7633-7637.
52. Otzen, D. E., Kristensen, O., Proctor, M. & Oliveberg, M. (1999). Structural changes in the transition state of protein folding: alternative interpretations of curved chevron plots. *Biochemistry*, **38**, 6499-6511.
53. Silow, M., Tan, Y.-J., Fersht, A. R. & Oliveberg, M. (1999). Formation of short-lived protein aggregates directly from the coil in two-state folding. *Biochemistry*, **38**, 13006-13012.
54. Babul, J. & Stellwagen, E. (1971). The existence of heme-protein coordinate-covalent bonds in denaturing solvents. *Biopolymers*, **10**, 2359-2361.
55. Muthukrishnan, K. & Nall, B. T. (1991). Effective concentrations of amino acid side-chains in an unfolded protein. *Biochemistry*, **30**, 4706-4710.
56. Pierce, M. M. & Nall, B. T. (1997). Fast folding of cytochrome *c*. *Protein Sci.* **6**, 618-627.
57. Colón, W., Wakem, L. P., Sherman, F. & Roder, H. (1997). Identification of the predominant non-native histidine ligand in unfolded cytochrome *c*. *Biochemistry*, **36**, 12535-12541.
58. Lambeth, D. O., Campbell, K. L., Zand, R. & Palmer, G. (1973). The appearance of transient species of cytochrome *c* upon rapid oxidation or reduction at alkaline pH. *J. Biol. Chem.* **248**, 8130-8136.
59. Harbury, H. A. & Loach, P. A. (1960). Interaction of nitrogenous ligands with heme peptides from mammalian cytochrome *c*. *J. Biol. Chem.* **235**, 3646-3653.
60. Zwanzig, R. W. (1997). Two-state models of protein folding kinetics. *Proc. Natl Acad. Sci. USA*, **94**, 148-150.
61. Hagen, S. J. & Eaton, W. A. (2000). Two-state expansion and collapse of a polypeptide. *J. Mol. Biol.* **297**, 781-789.
62. Pierce, M. M. & Nall, B. T. (2000). Coupled kinetic traps in cytochrome *c* folding: His-heme misligation and proline isomerization. *J. Mol. Biol.* **298**, 955-969.
63. Roder, H. & Elöve, G. A. (1994). Early stages of protein folding. In *Mechanisms of Protein Folding: Frontiers in Molecular Biology* (Pain, R. H., ed.), pp. 26-55, Oxford University Press, New York.
64. Qi, P. Q., Sosnick, T. R. & Englander, S. W. (1998). The burst phase in ribonuclease A folding: solvent dependence of the unfolded state. *Nature Struct. Biol.* **5**, 882-884.
65. Bhuyan, A. K. & Udgaonkar, J. B. (1999). Relevance of burst phase changes in optical signals of polypeptides during protein folding. In *Perspectives in Structural Biology* (Vijayan, M., et al., eds), pp. 293-303, University Press (India) Limited, Hyderabad.
66. Akiyama, S., Takahashi, S., Ishimori, K. & Morishima, I. (2000). Stepwise formation of α -helices during cytochrome *c* folding. *Nature Struct. Biol.* **7**, 514-520.
67. Chen, E., Wittung-Stafshede, P. & Kliger, D. S. (1999). Far-UV time-resolved circular dichroism detection of electron-transfer-triggered cytochrome *c* folding. *J. Am. Chem. Soc.* **121**, 3811-3817.
68. Barron, L. D., Hecht, L. & Wilson, G. (1997). The lubricant of life: a proposal that solvent water promotes extremely fast conformational fluctuations in mobile heteropolypeptide structure. *Biochemistry*, **36**, 13143-13147.
69. Bhuyan, A. K. & Udgaonkar, J. B. (1998). Multiple kinetic intermediates accumulate during the unfolding of horse cytochrome *c* in the oxidized state. *Biochemistry*, **37**, 9147-9155.
70. Clarke, J., Itzhaki, L. S. & Fersht, A. R. (1997). Hydrogen exchange at equilibrium: a short cut for analysing protein-folding pathways? *Trends Biochem. Sci.* **22**, 284-287.
71. Clarke, J., Itzhaki, L. S. & Fersht, A. R. (1998). A reply to Englander & Woodward. *Trends Biochem. Sci.* **23**, 3798-381.

72. Fersht, A. R. (1993). Protein folding and stability: the pathway of folding of barnase. *FEBS Letters*, **325**, 5-16.
73. Laurents, D. V., Bruix, M., Jamin, M. & Baldwin, R. L. (1998). A pulse-chase-competition experiment to determine if a folding intermediate is on or off-pathway: application to ribonuclease A. *J. Mol. Biol.* **283**, 669-678.
74. Bai, Y. (1999). Kinetic evidence for an on-pathway intermediate in the folding of cytochrome c. *Proc. Natl Acad. Sci. USA*, **96**, 477-480.
75. Camacho, C. J. & Thirumalai, D. (1993). Kinetics and thermodynamics of folding in model proteins. *Proc. Natl Acad. Sci. USA*, **90**, 6369-6372.
76. Gutin, A. M., Abkevich, V. I. & Shakhnovich, E. I. (1995). Is burst hydrophobic collapse necessary for protein folding? *Biochemistry*, **34**, 3066-3076.
77. Miller, R., Danko, C. A., Fasolka, M. J., Balazs, A. C., Chan, H. S. & Dill, K. A. (1992). Folding kinetics of proteins and copolymers. *J. Chem. Phys.* **96**, 768-780.
78. Sali, A., Shakhnovich, E. & Karplus, M. (1994a). How does a protein fold? *Nature*, **369**, 248-251.
79. Sali, A., Shakhnovich, E. & Karplus, M. (1994b). Kinetics of protein folding - a lattice model study of the requirements for folding to the native state. *J. Mol. Biol.* **235**, 1614-1636.
80. Skolnick, J. & Kolinski, A. (1990). Simulations of the folding of a globular protein. *Science*, **250**, 1121-1125.
81. Guo, Z., Thirumalai, D. & Honeycutt, J. D. (1992). Folding kinetics of proteins: a model study. *J. Chem. Phys.* **97**, 525-535.
82. Honeycutt, J. D. & Thirumalai, D. (1990). Metastability of the folded states of globular proteins. *Proc. Natl Acad. Sci. USA*, **87**, 3526-3529.
83. Hamada, D., Segawa, S.-I. & Goto, Y. (1996). Non-native alpha-helical intermediate in the refolding of beta-lactoglobulin, a predominantly beta-sheet protein. *Nature Struct. Biol.* **3**, 868-873.
84. Troullier, A., Reinstädler, D., Dupont, Y., Naumann, D. & Forge, V. (2000). Transient non-native secondary structures during the refolding of alpha-lactalbumin detected by infrared spectroscopy. *Nature Struct. Biol.* **7**, 78-86.
85. Pace, C. N. (1986). Determination and analysis of urea and guanidine hydrochloride denaturation curves. *Methods Enzymol.* **131**, 266-280.
86. Santoro, M. M. & Bolen, D. W. (1988). Unfolding free energy changes determined by the linear extrapolation method. Unfolding of phenylmethanesulfonyl alpha-chymotrypsin using different denaturants. *Biochemistry*, **27**, 8063-8068.
87. Tanford, C. (1970). Protein denaturation. C. Theoretical models for the mechanism of denaturation. *Advan. Protein Chem.* **24**, 1-95.
88. Chen, B., Baase, W. A. & Schellman, J. A. (1989). Low-temperature unfolding of a mutant of phage T4 lysozyme. 2. Kinetic investigations. *Biochemistry*, **28**, 691-699.

Edited by C. R. Matthews

(Received 3 May 2001; received in revised form 30 July 2001; accepted 6 August 2001)